AD-A209 997

SECURITY CLASSIFICATION OF THIS PAGE (When Data Entered)

REPORT DOCUMENTATION PAGE

READ INSTRUCTIONS BEFORE COMPLETING FORM

1. REPORT NUMBER: AFOSR-TR- 89-0912
2. GOVT ACCESSION NO.
3. RECIPIENT'S CATALOG NUMBER

4. TITLE (and Subtitle): SUPERPLASTICITY - A FUNDAMENTAL INVESTIGATION ON DEFORMATION MECHANISM AND CAVITATION PHENOMENA
5. TYPE OF REPORT & PERIOD COVERED: 2/1/86 to 1/31/89 final
6. PERFORMING ORG. REPORT NUMBER

7. AUTHOR(s): A.K. MUKHERJEE AND T.R. BIELER
8. CONTRACT OR GRANT NUMBER(s): AFOSR-86-0091

9. PERFORMING ORGANIZATION NAME AND ADDRESS: DIV. OF MATERIALS SCIENCE AND ENGINEERING, DEPT. OF MECHANICAL ENGINEERING, Univ. of California/Davis, CA
10. PROGRAM ELEMENT, PROJECT, TASK AREA & WORK UNIT NUMBERS: 6-1102F, 2306/A1

11. CONTROLLING OFFICE NAME AND ADDRESS: DR. ALAN ROSENSTEIN (202) 767-4933, AFOSR/NE, BUILDING 410, BOLLING AIR FORCE BASE, D.C. 20332-6448
12. REPORT DATE: JUNE 1989
13. NUMBER OF PAGES

14. MONITORING AGENCY NAME & ADDRESS(if different from Controlling Office): AFOSR/NE, Bldg. 410, Bolling AFB, DC 20332-6448
15. SECURITY CLASS. (of this report): UNCLASSIFIED
15a. DECLASSIFICATION/DOWNGRADING SCHEDULE

16. DISTRIBUTION STATEMENT (of this Report): UNLIMITED

DTIC ELECTE JUL 11 1989 S D

17. DISTRIBUTION STATEMENT (of the abstract entered in Block 20, if different from Report): UNLLIMITED

18. SUPPLEMENTARY NOTES: TO BE PUBLISHED IN MATERIALS SCIENCE AND ENGINEERING AND SCRIPTA METALLURGICA, AND JOURNAL OF MATERIALS SCIENCE.

19. KEY WORDS (Continue on reverse side if necessary and identify by block number): SUPERPLASTICITY, MECHANICAL BEHAVIOR, DEFORMATION MECHANISMS, CAVITATION PHENOMENON, ADIABATIC HEATING, THRESHOLD STRESSES, DISPERSION STRENGTHENING.

20. ABSTRACT (Continue on reverse side if necessary and identify by block number)

Superplasticity at high strain rates was obtained in mechanically alloyed aluminum IN90211. The high rate was due to the fine grain size. A threshold stress analysis, combined with SEM and TEM observations permitted the deformation mechanisms to be determined. Very little cavitation was observed, due to the grain morphology, and the deformation mechanisms that are operative.

DD FORM 1 JAN 73 1473

SECURITY CLASSIFICATION OF THIS PAGE (When Data Entered)

89 7 11 018

FINAL SCIENTIFIC REPORT

GRANT - AFOSR-86-0091

Period 2-1-86 TO 1-31-89

Superplasticity - A Fundamental Investigation on Deformation Mechanism and Cavitation Phenomena

by

Professor A. K. Mukherjee and T. R. Bieler
Division of Materials Science and Engineering
Department of Mechanical Engineering
University of California
Davis, California 95616

to

Dr. Alan Rosenstein
Air Force Office of Scientific Research
AFOSR/NE
Building 410
Bolling Air Force Base
D.C. 20332-6448

June 1989

ABSTRACT

The tensile behavior of mechanically alloyed (dispersion strengthened) IN90211 was characterized at strain rates between 0.0001 and 340/sec at temperatures between 425 and 475°C. At strain rates above 0.1/sec, superplastic elongations were obtained (maximum elongation 525% at 475°C, 2.5/sec). An unusual drop in the elongation-strain rate relationship was found to occur as a result of conduction of adiabatically generated heat in the deforming specimen. Large elongations were possible due to the lack of cavitation. Cavitation was precluded by the morphology of the grains and the high homologous temperature of deformation, that permitted high lattice diffusivity and easy climb of lattice dislocations over particles.

The data were analyzed assuming threshold stresses resist dislocation motion. The stress-strain rate data were linearized assuming n=2 (grain boundary sliding) or n=3 (solute drag) for the stress exponent. Both assumptions provided equally credible extrapolated values for a temperature dependent threshold stress between 5 and 10% of the Orowan bowing stress. The threshold stresses arise from a combination of local and general climb of dislocations over particles. Superplastic deformation was found to be dependent upon both grain boundary sliding and resistance of lattice dislocation motion. Consideration of the activation energies, details of flow behavior, and stress relaxation experiments provided stronger evidence for the n=3 solute drag mechanism to be the rate limiting process.

CONTENTS

I. THE SUPERPLASTIC DEFORMATION MECHANISMS OF IN90211 1
A. Experimental Details 3
B. Results 5
C. Analysis 9
D. Determination of the Threshold Stresses 10
E. Activation Energy 13
F. Discussion 15
1. Origin of threshold stresses for lattice dislocations 15
2. Origin of threshold stresses for boundary dislocations 19
3. Threshold stresses in IN9021(1) 21
4. The superplastic deformation mechanisms 23
G. Conclusions 30

References 32
TABLES 35
FIGURES 38

II. THE ROLE OF ADIABATIC HEATING ON HIGH RATE SUPERPLASTIC ELONGATION 46
A. EXPERIMENTAL PROCEDURE AND RESULTS 48
B. ANALYSIS 50
C. CONCLUSIONS 55

REFERENCES 56
TABLES AND FIGURES 57

III. CAVITATION OF MECHANICALLY ALLOYED ALUMINUM IN9021(1) AT 0.76-0.81 T_m 62
A. Experimental Procedure and Results 62
B. DISCUSSION 66
Deformation mechanisms 66
Grain Morphology 67
Mechanism of Cavitation 70
Fracture Surface 71
C. CONCLUSIONS 72

REFERENCES 74
TABLES and FIGURES 75

IV. CUMULATIVE LIST OF PUBLICATIONS RESULTING FROM AFOSR SUPPORT . 82

V. LIST OF PERSONNEL INVOLVED IN THE RESEARCH 87

I. THE SUPERPLASTIC DEFORMATION MECHANISMS OF IN90211

Creep and superplasticity have often been represented by the dimensionless equation first described by Mukherjee, Bird and Dorn [1]:

$$\frac{\dot{\varepsilon} kT}{DbG} = A\left(\frac{\sigma}{G}\right)^n \left(\frac{b}{d}\right)^p \qquad (1)$$

where $\dot{\varepsilon}$ is the minimum (usually steady state) strain rate, kT are Boltzman's constant times the absolute temperature, D is the dominant temperature dependent diffusivity. G is the temperature dependent shear modulus, and b is the Burgers vector. A is a mechanism-dependent constant, n is the stress exponent for the applied true stress σ, and p is the grain size exponent for the grain size d. The majority of the various theoretical models based upon micro-mechanical mechanisms for atom rearrangement by diffusion and dislocation motion, can be identified by specific constant values for D, A, n, and p.

IN90211 is a mechanically alloyed aluminum alloy that has a composition similar to 2124 aluminum alloys. In addition to the solution hardening provided by Mg atoms and the precipitation hardening provided by Cu in the form of θ phase, the mechanically alloying process introduces fine oxide and carbide dispersions [2,3]. The presence of these dispersions places this alloy in the class of metal matrix composites. IN90211 is nominally similar to IN9021, which has been described in the literature [4,5,6,7], but is slightly richer in alloying elements, as shown in Table 1. From the phase diagram, Mg is in solution at all temperatures, and a Mg enrichment by a factor of 2-3 at grain boundaries at high temperatures is expected [8,9]. Depending

upon the processing, θ precipitates can form as much as 5 vol% hard particles, in addition to the 5 vol% oxide and carbide dispersions.

IN9021(1) has exhibited superplasticity at unusually high strain rates [4,6,7,10]. The grain size associated with superplastic deformation mechanisms clearly affects the strain rate, assuming all other variables are equal in equation 1. Decreasing the grain size increases the superplastic strain rate. This has been demonstrated for a number of aluminum alloys with different grain sizes [11]. The submicron grain size of IN9021(1) is consistent with the high superplastic strain rates observed. Another feature of mechanically alloyed aluminum alloys is the extreme thermal stability of the grain size [12]. The lack of significant grain growth with strain and/or temperature makes the post forming properties IN9021(1) attractive, as they would be similar to undeformed material, (assuming cavitation is minimal). This alloy has been shown to have attractive tensile properties at room temperature, with high yield stresses and good tensile properties that can be modified by thermo-mechanical processing [7]. Unlike aluminum matrix composites with SiC whiskers, it is easily machined, and it has 10-15% tensile strains to failure.

This investigation focuses upon the deformation mechanisms that make these attractive technological results possible. The interaction between dislocations and the dispersions must be considered. Dispersions generally impose threshold stresses which must be exceeded for dislocations to overcome particles. At temperatures where diffusion is slow compared to the dispersion size and strain rate, the dislocations must overcome the particles by Orowan looping, which contributes to their strength. At elevated temperatures, where

diffusion becomes a significant factor in creep deformation, dislocations may overcome particles by a variety of climbing mechanisms that have been investigated in the past decade. These climb processes usually cause a threshold stress below that of the Orowan stress, often near half of that value, though smaller values are possible. Several significant advances in understanding the role of dispersions in creep deformation have been published in the past decade, describing local climb [13,14,15], general and cooperative climb [15,16], grain boundary dislocation interactions with particles [17,18,19], and the role of the interface between the particle and the matrix or grain boundary [2,18,20]. These considerations may affect the grain boundary sliding phenomena usually associated with superplasticity [21]. Furthermore, the apparent activation energies of dispersion strengthened materials are usually found to be several times larger than the activation energy for bulk diffusion. These concepts are discussed as they pertain to the deformation mechanism that permits the high strain rate superplasticity observed in IN9021(1).

A. Experimental Details

The specimens were machined from a processed sheet of IN90211. The sheet was made from an extruded rod provided by Novamet Aluminum lot 85V032 (currently available from Incomap, VA, and designated AL9021). The rod was forge flattened, and rolled in several successive passes at elevated temperature. Finally, the sheet was annealed at 492°C for an hour and water quenched. The specimen gage length was nominally 2.5 mm square cross section, and 6.4 mm long, with the tensile axis parallel to the rolling direction. The surfaces were sanded to 600 grit, and one

side was polished, and then scratched in the longitudinal direction, to provide reference for grain boundary sliding observations. Marks were made with a pencil on the other side to permit measurement of local strain. Specimens were photographed before and after testing to permit accurate area reduction measurements.

The tensile experiments were conducted in air in a hydraulic testing machine and heated in a radiant furnace. In all but the lowest two strain rates, the specimen was pulled within 10 minutes of reaching the test temperature. The temperature gradient along the gage length was usually within 3°C. Tests conducted at strain rates below 1/sec were conducted at constant true strain rate (assuming constant volume and uniform deformation), but computer control limitations required faster experiments to be done at constant displacement rate. The data were later converted to provide the true stress, strain and strain rate as a function of strain, described in more detail in [22]. Due to the high strain rate of the experiments, adiabatic heating occurred. The conduction of adiabatically generated heat away from the deforming zone affected the temperature profile of the deforming specimen, and substantially affected total elongation in some cases [22] (see Section II).

Several creep experiments were performed on IN9021 specimens to determine the low strain rate behavior of IN9021. Specimens deformed at creep rates above 10^{-7} were done on a hydraulic testing machine programmed to hold the specimen under constant stress. Since the rupture strains were usually less than 4%, lower creep rate experiments were done in a dead loading machine with constant load. Extensometers were used, providing strain measurement accuracy within 0.5%. Two

experiments with stress changes, and two experiments with temperature changes in the secondary creep regime were conducted to determine creep transient behavior and activation energy.

Load relaxation experiments were conducted to determine whether a threshold stress plateau appeared in the unloading behavior. The hydraulic testing machine was ill-suited for a formal load relaxation experiment, so only the terminal stress data were found to be useful. The load relaxation experiments were conducted by straining a specimen to about 25% elongation, and then the terminal stress was noted after two or more days of relaxation. Two of the three experiments were done with 50 mm long IN9021 specimens in an attempt to obtain better resolution. The difference in the composition and actual (uncertain) processing history resulted in the IN9021 specimens being stronger than the IN90211 specimens, but the deformation trends of both alloys were essentially the same.

Deformed specimens were investigated in optical, SEM and TEM for information regarding cavitation, fractography and grain boundary sliding, and microstructure [22] (Section III). One specimen was analyzed in X-ray diffraction in a Siemens x-ray diffractometer, and some information about residual stresses, texture change and precipitate formation was obtained [22].

B. Results

The results of the tensile tests are shown in Figure 1 and tabulated in Table 2. Figure 1a shows the elongation to failure as a function of strain rate, and Figure 1b shows the corresponding stress. As is usually observed in superplasticity [21] the stress-strain rate

behavior has a sigmoidal character, with maximum elongation occurring in the middle regime, where the strain rate sensitivity is high. However, the elongation dip in the middle of the superplastic regime is unusual, and has been analyzed in Section II, and found to be due to conduction of adiabatically generated heat. The dip in elongation is strictly due to the effect of heat conduction on flow stability, and does not represent a new microstructural phenomena. It is noteworthy that at the strain rates where many superplastic alloys have maximum elongation [11], IN9021(1) has poor elongation. These results are consistent with the IN9021 result of [4], but the IN9201 has a higher flow stress. The effect of adiabatic heating has not been observed in superplasticity before, and it is due to the unusually high strain rates of deformation for this alloy.

The stress vs. strain rate data of Figure 1b can be represented by the formula $\sigma = K\dot{\varepsilon}^m$, which is merely a rearrangement of equation 1 with m=1/n and K a constant. The strain rate sensitivity, m, is commonly near 0.5 (n=2) for superplastic materials and deformation mechanisms [23]. In the case of IN90211, m ≈0.25 (n=4), a value unassociated with superplasticity, but commonly representative of diffusional climb creep mechanisms [24,25]. At higher stresses, there is an apparent change to m≈0.15, (n≈7), but the data are few enough to be uncertain of their slope. At lower stresses, m<0.03, (n>33), and the transition appears to be rather abrupt. The high stress exponent is consistent with the high values observed in many dispersion strengthened alloys [5,24,26].

A family of stress-strain curves are shown in Figure 2. At low strain rates, the flow curve is smooth, but at higher strain rates, the flow curve is serrated when the true stress is between 25 and 75 MPa.

Serrations in the flow curve were also observed in the room temperature solution treated IN9021 work of Bane [7]. In the specimens deformed under constant true strain rate (up to 1/sec), the stress reached a plateau, and then decreased slightly with strain until necking commences. The effect of the decreasing true strain rate resulting from the constant displacement tests are evident in the flow curves from the higher strain rate experiments.

The creep data from IN9021 are compared with the IN9021 results of Kucharova, et. al. [5], Nieh, et. al. [4] and the IN9052 results of Otsuka et. al. [27], in Figure 3. Creep curves were typical, showing primary, secondary and tertiary stages similar to those observed by Otsuka and Kucharova. The data all show a similar trend of high stress exponents at strain rates below 10^{-3}/sec. At strain rates below about 10^{-6}, the stress exponent decreases to a value between 10 and 20. Comparison of the 475°C data of this study are in agreement with the Kucharova data. The stress change experiment shown in Figure 4 indicate inverse creep transients. Creep data from this study are tabulated in Table 3.

The results from X-ray diffraction showed large X-ray intensity peaks for aluminum, and many small diffraction peaks relating to precipitates, dispersions, and other unidentified compounds [22]. The tensile axis of the specimens were oriented perpendicular to the plane of the diffracting X-ray source and detector. The relative intensity of the aluminum diffraction peaks differed from a standard powder specimen as tabulated in Table 4.

The IN90211 peaks are compared to the powder specimen in the ratios under the columns headed by I/I_{Al}. The relative intensity of the (111)

peaks was the same as in the powder specimen, but the relative intensities were higher for the other reflections in the IN90211 specimens, indicating that texture is present in the alloy. The (200) peak intensity for the undeformed specimen was 1.3 times higher and 2.1 times higher for the deformed specimen, indicating that the texture present in the undeformed specimen was increased as a result of superplastic deformation. The high intensities of the (200) planes indicates that there is a preferential alignment of {001} poles parallel to the tensile axis. This orientation puts a higher than usual number of (111) planes, where slip occurs, in an orientation nearer 35° to the tensile axis, where they would be oriented closer to the planes of maximum shear. In this orientation the number of (111) planes diffracting toward the detector would be relatively reduced.

The results of microscopic investigations of specimens deformed superplastically are as follows: Fracture surfaces were intergranular, having features ranging in size from 0.2 to 3 μm. Measurable cavitation was observed within 1 mm of the fracture surface only in specimens that did not deform superplastically (Section III). Grain boundary sliding of 2-3μm clusters of grains was observed in SEM. In TEM, the grain size was found to be submicron, and unaffected by long term stress and temperature (e.g. 475°C, 10 MPa, 2.6 Msec). The dispersions were observed to reside in both the boundaries and grain interiors and their size and interaction with dislocations was noted. Particles were spherical, and varied from 7 to 25 nm in diameter, with an average diameter of 15 nm. Dislocations were found to be pinned to particles, with little or no bowing between the particles, indicating that the dislocations were attracted to the particles. The particle spacing

along a dislocation line was typically between 20 and 80 nm, with an average spacing of 45 nm. These values agree with the calculated particle volume of 5-6 vol%. Grain boundary dislocations were observed on both high and low angle boundaries. Low angle boundaries are readily found, and can be interpreted as being stable subgrain boundaries within the 2-3 μm clusters of subgrains. Details are found elsewhere [22,28].

C. Analysis

Threshold stresses have been invoked to explain the unusually high apparent stress exponents of dispersion strengthened materials. This is evident in the analysis of deformation behavior of mechanically alloyed aluminum [5,25,27], and nickel based alloys [24,29]. In this case, a stress exponent is assumed, generally n=4 for dislocation climb creep, and the data are analyzed to determine the threshold stresses that would cause the true stress exponent to be n=4. In the case where superplastic deformation mechanisms are suspected, an apparent stress exponent of n=4 could be the result of a n=2 deformation mechanism (for grain boundary sliding mechanisms [23], that is affected by threshold stresses.

Since threshold stresses are usually reported in terms of the Orowan stress, it was determined from the particle spacings based upon the volume fraction and the measured particle size.

$$\sigma_0 = 0.84bG/L \approx 180 \text{ MPa}. \qquad (2)$$

This stress corresponds to the stress where the transition between the superplastic and high stress regime is observed in Figures 1 and 3.

Therefore, if lattice dislocations move past particles in the superplastic regime, they must do so by climb, rather than Orowan looping. A stress exponent of 7 has also been reported in situations where climb and annihilation of Orowan loops is the probable deformation mechanism [1].

The data were analyzed according to the following strategy: Threshold stresses were determined from a linear extrapolation of the superplastic data to zero strain rate; they were found to depend upon temperature and the assumed values for the stress exponent n. When threshold stresses are present, the stress in equation 1 refers to the internal effective stress, σ_f; $\sigma_f = \sigma_a - \sigma_o$, where σ_a is the applied stress and σ_o is the threshold stress. The threshold stresses were subtracted from the applied stress data to obtain effective stresses which could be analyzed to obtain the true activation energy for the superplastic process. Also, the activation energy of the threshold stresses was determined.

D. Determination of the Threshold Stresses

Threshold stresses, if present, affect the apparent stress exponent in the logarithmic plots of strain rate vs. stress [24,26]. As the applied stress decreases, the apparent stress exponent increases as the applied stress approaches the threshold stress. The extrapolation procedure used to obtain the threshold stresses is well documented in the literature [24,30]. Implicit in this method of extrapolation is the unfortunate but unavoidable introduction of an assumed stress exponent value into the data. Once this is done, the data lose their objectivity, so any interpretations of the affected data should be

substantiated by other observations as well. For example the IN90211 UTS data are shown in Figure 5, extrapolated under the three values of the stress exponent of n=2, 3 and 4. These values were chosen since there are many theoretical models predicting stress exponents with these values. The data were not linear for n=4, so this extrapolation was discounted. (If the n=4 data were linear, then threshold stresses could not exist, since the apparent stress exponent was n≈4.) The data for n=2 and n=3 were both reasonably linear, providing a different set of temperature dependent threshold stress values, so both interpretations are considered.

The superplastic data were extrapolated to zero strain rate using a linear regression analysis for the data at each of the five experimental testing temperatures. There were 4 and 7 data for the 425 and 475°C superplastic data, respectively. The 438, 450 and 462°C superplastic only had 2 data at each temperature, so the extrapolation for these temperatures is less accurate. Values for these middle temperatures were modified on the basis of the activation energy analysis of the threshold stress described below. In addition the UTS data in Figure 5, regression analyses were done at the maximum true stress ($.2<\varepsilon<.3$), $\varepsilon=0.3$, and $\varepsilon=0.5$, (tabulated in Table 2) to determine how strain affected the threshold stress value. Since adiabatic heating occurred in the deforming specimens at higher strain rates, a correction to the stress (based upon the apparent activation energy of the superplastic data) was made assuming the test could have been accomplished isothermally. The details of this analysis are described elsewhere [28]. Figure 6 shows how the threshold stress increased slightly with increasing strain. As the amount of increase was not much larger than

the experimental error, an average value was used in subsequent analysis; these threshold stresses (tabulated in Table 5), are in the range of 1.5-15% of the Orowan stress.

The n=2 and n=3 extrapolated threshold stresses correlate with two different means of determining the threshold stress. The three load relaxation experiments provided estimates of the threshold stress at three different temperatures that agree with the n=3 analysis (shown in Table 5). The load relaxation value obtained on the IN90211 specimen at 450°C, 9±2 MPa is slightly higher than the extrapolated n=3 6.8 MPa value. This difference can be rationalized if the specimens did not completely relax in the two days. The other two load relaxation values were obtained on IN9021 specimens, which were stronger than IN90211 in the condition tested. Consequently, the extrapolated n=3 IN92011 threshold stresses do not agree as closely with the IN9021 load relaxation values, but the n=3 extrapolated values are much closer to the measured relaxation stress than the n=2 values.

The n=2 extrapolated values are in agreement with an empirical measure of the threshold stress indicated by creep data of IN9021 shown in Figure 3. The high stress exponent regime appears to be a transition between the superplastic deformation regime and a creep regime with a stress exponent of about 13. This transition occurs at a threshold stress of about 17 MPa at 475°C. This value is in agreement with (i.e. slightly larger than) the IN90211 n=2 extrapolated value of 16 MPa. The n=2 threshold stresses correlate with the lower limit of the superplastic deformation regime.

E. Activation Energy

The activation energy of the IN90211 and IN9021 data were obtained in two ways; an apparent activation energy over the large range of experimental stresses and strain rates, and an analysis of the true activation energy of the superplastic regime, taking into account n value assumptions, threshold stresses, and shear modulus corrections. The apparent activation energy was determined by taking the natural logarithm of both sides of the empirical equation

$$\dot{\varepsilon} = A\sigma^n \exp(-Q_a/RT). \qquad (3)$$

At constant values of stress, the term with the stress exponent drops out, and the Arrhenius plot illustrated in Figure 7 for several stress values provides the apparent activation energy. At very high stress values (where the effect of the threshold stress is negligible), the apparent activation energy is 135±10 kJ/mol. At lower stresses, where superplasticity occurs, the apparent activation energy increases to about 155±10 kJ/mol. Both of these values are close to the lattice diffusion activation energy of 142-145 kJ/mol reported for pure aluminum [31]. Below the superplastic regime, the apparent activation energy increases precipitously to a value between 1000 and 2000 kJ/mol, but the value returns gradually to lower values with decreasing stress, approaching the high stress value. The stress where the activation energy increases corresponds to the n=2 threshold stress values. This change suggests a transition between two deformation mechanisms with activation energies near lattice diffusivity, rather than a separate deformation mechanism with a huge activation energy. The true

activation energy was obtained by taking the natural logarithm of equation 1, taking into account the threshold stresses. This equation becomes

$$\begin{matrix} \mathrm{Ln}(\dot{\varepsilon}) - n\mathrm{Ln}(\sigma_a - \sigma_o) - \mathrm{Ln}(A'D_o b) \\ + (n-1)\mathrm{Ln}(G) + \mathrm{Ln}(T) \end{matrix} = \frac{-Q}{RT} \qquad (4)$$

where the term A′ contains the grain size dependence and the structural parameter A. The value used for G was G(T) = 30220 - 16T MPa [32]. All of the superplastic data at UTS are plotted according to equation 4 in Figure 8, with n=2 and n=3 threshold stress assumptions. The data did not all lie on the same collinear line, but they appear to vary somewhat with strain rate. However, the data were at nominally the same strain rates for the different temperatures, providing symmetry so that a linear regression of the data would provide the true activation energy (based upon the n value assumptions). A similar regression was accomplished at each of the four strains in Table 2, and the results of this analysis are given in Table 6. As with the value of the threshold stresses, the activation energy increased slightly with strain, so that average values were taken. These increases with strain suggest that the microstructure changes with strain, increasingly resisting dislocation motion. The true activation energy was 90±10 and 120±17 for the n=2 and n=3 assumptions, respectively. The n=3 activation energy value corresponds with the range of activation energies for the diffusivity of Mg in Al [31].

The activation energy of the threshold stress is plotted for the n=2 and n=3 cases in Figure 9. The paucity of data for the three middle temperatures is evident in their variation off of linearity in the Arrhenius plot. The activation energies for the n=2 case is 60 kJ/mol,

in agreement with reported values for grain boundary diffusion [33], and 140 kJ/mol for the n=3 case, in close agreement with reported 142-145 kJ/mol lattice diffusivity of aluminum [31]. These activation energies were derived by taking a linear regression of the extrapolated threshold stress data from Figure 5. The threshold stress values for the middle three temperatures were modified to be collinear with the 425 and 475 data on the Arrhenius plot. These modified threshold stress values are the ones given in Table 5.

F. Discussion

From the values of the threshold stress and activation energies, the origin of the threshold stress can be determined. With the use of other experimental observations, the probable deformation mechanisms are determined for the superplastic deformation of IN90211.

1. Origin of threshold stresses for lattice dislocations

Threshold stresses resulting from climb of dislocations climbing over particles generally arise from the increase in the energy of the dislocation line required for bypassing. This process has been theoretically investigated, describing local climb [13, 34], cooperative climb [15,16], and general climb [16,34,35]. Since precipitates and particles are generally harder than the surrounding matrix, dislocations are repelled from particles lying the slip plane, forcing the dislocation to climb over the particle (if the stress is below the Orowan stress) [14]. In this case, the dislocations do not interact with the particle interface, as illustrated by the general climb schematic in Figure 10. When the particle volume fraction is high,

dislocations climb around the particles in a cooperative way, finding a minimum energy path though the obstacles. Local climb has been observed in dispersion strengthened alloys, where the interface between the dispersion and the matrix is incoherent. At elevated temperatures, diffusion permits relaxation of the interface in such a way that shear and tensile tractions across the interface are reduced, or vanish. As a result of this, the interface becomes attractive to dislocations, providing a way to reduce their line energy [15,34]. Detaching the dislocation from the dispersion therefore requires a force to break the dislocation free from the relaxed interface, and the threshold stress arises from the departure side pinning such as that seen in Ni based alloys [15,24].

The magnitude of the threshold stress depends substantially on the particle size and spacing, and the character of the climbing process. The threshold stress is usually evaluated as a fraction of the Orowan stress. Local climb theory predicts that threshold stresses are approximately half of the Orowan stress [13,34]. Local climb threshold stresses are not dependent upon lattice diffusion but on the diffusivity in the particle/matrix interface. If there is sufficient temperature for diffusion in the interface, more diffusivity in the interface does not substantially increase the attractiveness of the interface for dislocations. Therefore local climb threshold stresses are nominally invariant with temperature or stress, and can be represented by

$$\dot{\varepsilon} \propto (\sigma-\sigma_o)^n. \qquad (5)$$

The effect of a constant stress is to cause a smooth asymptotic approach

to the threshold stress with decreasing strain rate as illustrated in Figure 11. The apparent stress exponent therefore increases smoothly toward infinity.

On the other hand, the effect of diffusion (and thus temperature) on the magnitude of threshold stresses is strong in general climb. As illustrated in Figure 10, the length of the dislocation line in general climb is shorter than for local climb, so less energy is needed to create the extra dislocation length. Also, the bending radius of the dislocation line is more severe in the local climb case, so a larger stress is needed to maintain that bend. Consequently, general climb threshold stresses are lower than local climb threshold stresses (often by an order of magnitude for low particle fraction alloys [34]). The dislocation curvature depends also upon the particular interaction of dislocation velocity, diffusivity (strain rate and temperature) and the applied stress. Higher applied stresses cause higher threshold stresses due to the increased dislocation velocity, which decreases the time for diffusion, which decreases the curvature radius and increases the length of the dislocation. The value of the threshold stress in general climb conditions also depends upon the volume fraction of the particles [34]. Dislocation progress by general climb depends explicitly on this balance between lattice diffusion and the applied stress. Analysis of general climb indicates that general climb causes a resisting stress proportional to the applied stress, characterized by [16,24]

$$\dot{\varepsilon} \propto (\sigma - k\sigma)^n = (1-k)^n \sigma^n, \qquad (6)$$

so that no apparent change in the stress dependence results from the

threshold stress. Therefore general climb threshold stresses are more difficult to quantify than local climb thresholds stresses.

A mixture of general and local climb is possible. Arzt, et.al. [36] have defined a stress relaxation parameter κ, such that

$$\sigma_* = \sigma_0(1-\kappa^2)^{1/2}, \tag{7}$$

where σ_0 is the Orowan stress. The stress relaxation parameter describes the degree to which the interface is relaxed. The relaxation parameter is related to the angle between the particle and the dislocation line at the interface, analogous to an equilibrium wetting angle, and defined by

$$\cos \phi = \kappa. \tag{8}$$

For a typical threshold stresses of half the Orowan stress, the relaxation parameter is 0.866 (ϕ=30°), indicating that the interface is only slightly relaxed. The value of this parameter indicates that local climb only occurs for the part of the particle passing event where the equilibrium angle is at or smaller than the equilibrium value of ϕ. With a partially relaxed interface, a mixture of general and local climb results, as illustrated in Figure 12a.

In summary, the incoherent interfaces of dispersion strengthened materials can relax at sufficiently temperatures, causing the interface to become attractive to dislocations. The degree of attraction is determined by several factors, such as the nature of the interface, the shape of the particle, the temperature, and the Orowan Stress (which is

dependent on the particle size and concentration). Therefore a continuum between local and general climb is possible, and therefore a curve with behavior between the two extremes shown in Figure 11. The degree to which a particle passing event is local or general depends upon these factors. Consequently, the threshold stress may be relatively constant if local climb characteristics dominate, or smaller, and dependent upon stress and temperature, if general climb characteristics dominate.

2. Origin of threshold stresses for boundary dislocations

Grain boundary sliding is nearly always observed in superplastic deformation [21]. Grain boundary dislocations are generally involved in the theoretical treatments of superplastic deformation processes [23]. Regardless of the source of grain boundary dislocations, they must be mobile for grain boundary sliding to occur. Boundaries must be high angled [37], and for dispersion strengthened materials to be superplastic, grain boundary dislocations must be able to overcome particles in the boundary.

Particles in the boundary have been noted to resist the progress of grain boundary dislocations [38]. The geometry and chemistry of the grain boundary region is more complicated than the lattice. This has been addressed for dispersion strengthened materials, and is commonly called interface controlled diffusional creep [2,18,20]. Threshold stresses arise in the interface in analogous ways as in the lattice, and in also in some ways that are particular to the interface(s). Geometrically based threshold stress predictions have been derived, [18,39], but since these values vary with temperature only

by the variation of the shear modulus, they appear irrelevant to the this investigation. The creep described by the very complicated relation in aav can fortunately be dismissed since the homologous temperatures of this investigation (0.74-0.80) are sufficiently high so that lattice diffusivity dominates diffusion. Therefore only the threshold stress theories that are analogous to the local and general climb described for the lattice will be considered further.

Assuming that grain boundary dislocations overcome particles in the boundary by climbing processes, the boundary threshold stresses differ from the lattice threshold stresses in proportion to the differences in their structural properties. The Burgers vector for grain boundary dislocations depends upon the nature of the grain boundary; whether it is low or high angled. High angle grain boundary Burgers vector can be estimated as one third of the lattice Burger's vector [18]. Similarly, an estimate of the shear modulus of the boundary can be obtained considering the difference between the thermal expansion in a polycrystal compared to a single crystal. This has been done for copper, and the expansion coefficient derived for the grain boundary is 2-5 times larger than the bulk [40]. Since expansion is a measure of elastic bond strength, the shear modulus in the boundary can be estimated to be about one third of the bulk. Using the estimates of grain boundary Burgers vector and shear modulus in the Orowan bowing equation (2), the boundary Orowan stress is about an order of magnitude smaller than that in the bulk. If local climb phenomena occur in the boundary then the local climb threshold stress can be estimated at about half the boundary Orowan stress for the IN9021(1) alloys (9 MPa), a value that is in the range of the n=3 threshold stress values given in

Table 5.

The discussion regarding the mixed local and general climb for the bulk does not immediately carry over into the boundary, for geometric reasons. It is difficult to imagine how any kind of general climb phenomena can occur if a boundary dislocation is constricted to remain in the plane of the boundary. For this reason, boundary threshold stresses should be relatively insensitive to temperature once the temperature is sufficiently high to permit interfacial diffusion in the particle/matrix interface. Since this result does not agree with the temperature sensitivity obtained in the above analysis, it appears that these threshold stresses do not arise in the grain boundary. This does not mean that boundary threshold stresses do not exist, but only that they do not affect the rate limiting process of deformation.

3. Threshold stresses in IN9021(1)

The threshold stresses in IN9021(1) are smaller than those usually reported where local climb is invoked, since they are 1.5-15% of the bulk Orowan stress, instead of about half. These smaller threshold stresses can be rationalized as a mixture of local and general climb of lattice dislocations if general climb characteristics dominate the climb over the particles. The equilibrium angle ϕ for these small threshold stresses is small, between 1 and 10°. The presence of lattice diffusion and particle-dislocation attraction is apparent in the mixed climbing over particles in the IN90211 matrix in Figure 13. A schematic comparison between a large threshold stress and a smaller one, based upon 10% of the Orowan stress (and thus a 6° angle) is shown in Figure 12. Smaller equilibrium angles correspond with greater amounts of

lattice diffusion adjacent to the particle, and thus a larger dependence upon temperature (i.e. lattice diffusion). The equilibrium angle and thus the proportion of local climb phenomena decreases with increasing temperature, so the threshold stress decreases in accordance with the larger curvature and the shorter line length of the climbing dislocation. Since part of the dislocation is always in contact with the interface, due to its attraction, the climb process will never be completely general. No effect of the threshold stress on the apparent stress exponent would occur if climb was completely general. Therefore since some component of local climb is always present in this alloy (due to the attraction the interface has for the dislocation), the threshold stress will always have some effect on the apparent stress exponent.

The effect of local climb in the interface on the stress exponent decreases with the magnitude of the threshold stress, which decreases with increasing temperature. This explains why the apparent stress exponent is smaller for the 475° data than the 425° data in Figure 3. In cases where local climb is more dominant, the effect of the threshold stress is more apparent in causing a smooth curvature on the lower stress regime, as evident in the 425°C data of Figure 3. However, the abrupt change in mechanism that occurs when the superplastic deformation mechanism is shut down (at the n=2 threshold stresses) may obscure the smooth transition that could potentially be there, as suggested by the dashed line in Figure 11. From the abrupt change in the activation energy at the n=2 threshold stresses, the low stress regime illustrated in Figure 1 is not due to the effect of the threshold stresses in the way seen in other alloys, such as that of TD-Nichrome [26].

4. The superplastic deformation mechanisms

Deformation mechanisms associated with n=2 and n=3 are consistent with the observations of flow in the experiments. The majority of the superplastic deformation mechanisms have in common grain boundary sliding, predicting n=2. Most models assume that diffusion assists grain boundary migration and/or grain boundary dislocation motion to accommodate the stress concentrations arising in the sliding process. The differences depend upon what part of the dislocation and diffusion mechanisms are rate limiting. The models of Ball and Hutchinson, and Mukherjee [41,42,43], are represented by

$$\frac{\dot{\varepsilon} kT}{GD_{gb}b} = A \left(\frac{\sigma}{G}\right)^2 \left(\frac{b}{d}\right)^2, \qquad (9)$$

The Ball and Hutchinson model assumes that grains slide in clusters, providing A=200. The Mukherjee models assume individual grains slide, with A=2 or 75-150, depending upon the details of the climb process. They have in common dependence upon grain boundary diffusion, p=2, and n=2.

Sherby and co-workers have obtained empirical expressions that describe different dependence of grain size and diffusivities [44]. When grain boundary diffusion controls sliding, they obtained a grain size dependence of p=3.

$$\dot{\varepsilon} \approx 10^8 \frac{bD_{gb}}{d^3}\left(\frac{\sigma}{E}\right)^2 \qquad (10)$$

When lattice diffusion was rate limiting, they describe grain boundary sliding by

$$\dot{\varepsilon} \approx 2 \times 10^9 \frac{D_l}{d^2} \left(\frac{\sigma}{E}\right)^2 \tag{11}$$

for a number of materials. Experimental results generally give a grain size dependence of 2-3, and activation energies are usually near lattice or boundary diffusion. The details of the accommodation process for grain boundary sliding in actual materials varies, as do the theories.

The deformation mechanism most commonly associated with n=3 is dislocation glide limited by solute atoms residing in the dislocation cores [32,45], given by

$$\dot{\varepsilon}_g \approx \frac{\pi(1-\nu)kT\bar{D}}{6e^2 c_b^5 G}\left(\frac{\sigma}{G}\right)^3, \tag{12}$$

$$e = (\Omega^*/\Omega_b)^{1/3} - 1, \tag{13}$$

where c is the atomic concentration of the solute, c_b = 1-c is the atomic concentration of the solvent or bulk atoms, ν is Poisson's ratio, e is the solute-solvent size difference [45] (Ω^* is the effective atomic volume of the solute atom and Ω_b is the size of bulk atoms in pure state). $\bar{D}$ is the Darken diffusivity of the solute, which is essentially the same as Mg diffusivity in Al, since the concentration is small. When solute drag is observed to control dislocation motion, the flow curve can exhibit serrated flow at the higher stresses of the deformation regime. The stress corresponding to the breakaway of glide dislocations from solute atmospheres is given by [41]

$$\sigma_b = \frac{W^2 c,}{5b^3 kT} \tag{14}$$

$$W = \frac{-1}{2\pi}\left(\frac{1+\nu}{1-\nu}\right) G|\Delta V| \tag{15}$$

where W is the binding energy between the solute atom and the dislocation and ΔV is the difference in volume between the solute and solvent atoms. At stresses not greatly exceeding the breakaway stress, intermittent breakaway can occur. The dislocations occasionally break free from the solute atmospheres for a limited slip distance, causing the serrated flow curve (the Portevin-LeChatelier effect). A similar phenomena is predicted by Oliver and Nix [30] in dispersion strengthened alloys. When the curvature of a dislocation around a particle reaches a certain angle, the dislocation can break away from the solute atmosphere. For this alloy, the stress where this occurs is similar to that given above. As shown in Figure 4, The IN90211 data exhibit serrated flow at stresses greater than 20 MPa, which is in agreement with the above prediction.

Two other theories predicting n=3 include models based on dislocation climb, and a pipe diffusion controlled diffusional creep. The pipe diffusion model predicts strain rates so much lower than those observed, that it can be neglected. Weertman and Weertman [48] have shown that when glide and climb distances are similar, dislocation climb can occur with an n=3 rate law. It is given as

$$\frac{\dot{\varepsilon} kT}{D_l G b} \approx A\left(\frac{\sigma}{G}\right)^3, \tag{15}$$

where A is a constant between 1 and 25. The climb distance for dislocations is less than or equal to the radius of the particles, so it is less than 10 nm. The glide distance is about equal to the interparticle distance of 30-50 nm. These distances differ by less than an order of magnitude, so this model can apply to the flow of dislocations in IN90211. This is the theoretical basis for all climb theories, where details of substructure cause increases of the climb stress exponent from 3 up to values as large as 7.

When the n=2 and n=3 threshold stresses are subtracted from the applied stress, the data can be plotted using the effective stress in equation 1, and compared to the above theoretical predictions. This has been done for three cases using the IN90211 UTS data and diffusivity values given in Table 6 (Figure 13). In each case, the stress exponent of the data matches the chosen n value. This occurs because the threshold stresses were determined so that the data would follow the assumed n value.

Of all the terms in equation 1, the structure parameter A and the diffusivity are the least accurately known. For the n=2 effective stresses the grain boundary diffusivity was used, and for the n=3 effective stresses Al self diffusion, and Mg diffusion in Al were used. From the agreement between activation energies of the threshold stresses and activation energies for lattice and boundary diffusion, it seems unreasonable to plot n=2 effective stresses with the strain rate data normalized by lattice diffusion, as well as the converse case. The grain boundary diffusivity was taken from an estimate [49], which has been corroborated in part in later experimental results [33]. There is considerable scatter in the reported diffusivity of Mg in Al, covering

more that an order of magnitude [8]. Agreement between the data and the Cottrell-Jaswon model in Figure 13b was obtained with Mg diffusivities on the high end of the range. The diffusivity of Cu in Al is almost identical (in magnitude) with Al self diffusion, so the Cottrell-Jaswon theory with Cu solute atoms is plotted in Figure 13c where the data are normalized by lattice diffusivity. It is apparent that solute drag of Cu atoms does not limit the overall deformation of IN90211. For the plot of the Weertman model, the value of A=25 was used, which is the high limit of this term.

Agreement between the n=3 models and the data were obtained, but not for the n=2 models. One reason for the disagreement in the n=2 case is the lack of certainty in the pre-exponential frequency term for grain boundary diffusion. However, it seems difficult to attribute 7 orders of magnitude to this uncertainty. The serrations in the flow curves support the Cottrell-Jaswon solute drag theory, even though climb of dislocations clearly occurs, as demonstrated by the threshold stress analysis. Also, the inverted creep transients are consistent with glide limited dislocation motion. Therefore the n=3 models best describe the rate limiting flow mechanism of IN90211 as occurring in the grain interiors, rather than in the grain boundaries due to the sliding that was observed.

The Weertman model is based on lattice diffusivity rather than a Darken diffusivity, so the true activation energy of 120 kJ/mol obtained in the n=3 analysis is somewhat lower than the lattice diffusivity activation energy of 145 kJ/mol. The Weertman climb model predicts a true activation energy that is higher than the analysis provides. However, IN90211 dislocation cores contain Mg atoms, so it is plausible

that climb of dislocations could depend upon Mg diffusion, so that the Weertman model with Mg diffusivity would apply to this alloy. Introduction of this diffusivity value would cause the value of A to be lower to be in agreement with the IN9021l data.

The empirical lattice diffusivity limited grain boundary sliding relation of Sherby is in agreement with the rate of deformation, with a grain size of 3 μm, but the stress exponent is n=2. This correspondence suggests that the grain boundary sliding is dependent upon lattice diffusivity, and at a rate very similar to the n=3 mechanisms. With the 0.5μm grain size, the predicted strain rate is too fast, so from this result a reasonable description of the grain size is 3 μm, but consisting of stable submicron subgrains. Superplastic deformation of this alloy can therefore be described with all three deformation mechanisms occurring sequentially at very similar rates, but with the n=3 rates controlling the overall deformation process.

From these observations, the following superplastic deformation mechanism for IN9021(1) is proposed: Dislocation progress in the lattice is resisted by two forces, that of the diffusion of solute atoms in the dislocation cores, and the need to climb over particles. The high homologous temperature makes both lattice and solute diffusion easy and dominant, so though local climb would be expected, the slow dislocation progress permit increased general climb phenomena to occur. The departure side pinning resulting from the attractive interface of the particle account for the observable threshold stress. As dislocations arrive at the grain boundary, they encounter more Mg atoms, slowing their progress, permitting time for transformation into grain boundary dislocations. Though grain boundary dislocations can normally

move through the boundary with greater ease than bulk dislocations, due to the more open structure, their progress is resisted by the enriched Mg solute drag and the need to overcome particles in the boundary by strictly local climb. Since grain boundary dislocation progress can occur faster than the arrival of extrinsic dislocations, the threshold stresses arising in the boundaries do not affect the measured stress. The rate controlling mechanism determines this value, and thus grain boundary threshold stresses are not apparent in the superplastic data. The ease of slip in the grains permits accommodation of incompatibilities at triple joints and other obstacles, precluding cavity formation at stress concentrations. The grain boundary sliding permits grains to rotate toward orientations that make slip easier, as evidenced by the increase in texture that aligns slip planes preferentially for maximum shear.

The result of decreasing the stress below that of the n=2 threshold stress is to shut down the grain boundary sliding process. These threshold stresses are consistent with local climb threshold stresses in the boundary, though the reason for their temperature dependence is uncertain. When the grain boundary dislocations cannot accommodate the arrival of lattice dislocations at the boundary, then stress concentrations that can lead to cavitation can occur, and fracture results thereby.

This sort of a boundary threshold stress that affects grain boundary sliding has also been observed in a mechanically alloyed superalloy, MA6000 [29]. They proposed that the superplastic regime resulted from Coble creep occurring when stresses were high enough to overcome a temperature dependent threshold stress in the boundary. The

activation energy for the threshold stress was low, about 20% of the self diffusion activation energy. Their superplastic regime was too small to permit a threshold stress analysis, so they were limited to more speculative arguments too account for their data. This work has shown that an interpretation similar to theirs can result from a more rigorous analysis, since IN90211 provided sufficient data to analyze.

G. Conclusions

IN9021 shows considerable promise as a useful engineering alloy for superplastic forming. It has a high yield strength with good tensile properties. It can be superplastically formed at commercially attractive strain rates between 1 and 10/sec. Tensile elongation in excess of 500% were obtained in IN90211 mechanically alloyed aluminum at strain rates between 1 and 5/s at 475°C.

There was evidence for two temperature dependent threshold stresses associated with superplastic behavior. Unlike most dispersion strengthened alloys, the threshold stress associated with the rate limiting flow does not account for the observed low stress-low strain rate behavior. The low stress regime results from yet another threshold stress, associated with grain boundary dislocation and diffusion phenomena.

The threshold stresses associated with the rate limiting behavior arise from mixed local/general climb of lattice dislocations over particles and precipitates. The superplastic behavior at high strain rate is the result of the fine 3 μm grain clusters consisting of stable submicron subgrains pinned by particles. Grain boundary sliding was clearly observed, but analysis based on n=2 grain boundary sliding

models provided an inferior overall interpretation of the data when compared to an n=3 analysis. The n=3 analysis is consistent with the observed serrated flow resulting from intermittent dislocation breakaway from Cottrell atmospheres. Since the glide and climb distances of dislocations in the grains are similar in magnitude, the universal climb model of Weertman (having n=3) can also describe the flow of IN90211. The deformation occurs on the basis of grain boundary sliding mechanisms, but sliding is limited by the rate that lattice dislocations can arrive and dissociate into grain boundary dislocations in the boundary. Current superplastic theories do not fully account for the combination of lattice slip limited by solute drag and climb, and the grain boundary sliding observed in this alloy.

References

1. J.E. BIRD, A.K. MUKHERJEE, and J.F. DORN, Quantitative Relation Between Properties and Microstructure, Proceedings of International Conference in Haifa, Israel, Israel University Press, (1969), 255.

2. W.C. OLIVER and W.D. NIX, Acta Metallurgica, 30, (1982), 1335-47.

3. J.S. BENJAMIN and M.J. BOMFORD, Metallurgical Transactions, 8A (1977) 1301-1305.

4. T.G. NIEH, P.S. GILMAN, and J. WADSWORTH, Scripta Metallurgica, 19, (1985), 1375.

5. K. KUCHAROVA, A. ORLOVA, H. OIKAWA, and J. CADEK, Materials Science and Engineering A, 102, (1988), 201-209.

6. W.J.D. SHAW, Materials Letters, 4 (1985) 1.

7. S.J. BANE, J. BRADFIELD, and M.R. EDWARDS, Materials Science and Technology, 2, (1986), 1025-30.

8. C. LEA, and C. MOLINARI, "Magnesium diffusion, surface segregation and oxidation in Al-Mg alloys", Journal of Materials Science, 19, (1984), 2336.

9. T. MALIS and M.C. CHATURVED, J. Materials Science, 17, (1982), 1479.

11. A.H. CHOKSHI, T.R. BIELER, T.G. NIEH, J. WADSWORTH, and A.K. MUKHERJEE. In: Superplasticity in Aerospace, The Metallurgical Society (1988) 229-245.

12. J.A. HAWK and H.G.F. WILSDORF, Scripta Metallurgica, 22, (1988), 561-7.

13. R.S.W. SHEWFELT and L.M. BROWN, Philosophical Magazine, 35, 945-962.

14. D.J. SROLOVITZ, M.H. LUTON, R. PETKOVIC-LUTON, D.M. BARNETT and W.D. NIX, Acta Metallurgica, 32, (1984), 1079-88.

15. E. ARZT and M.F. ASHBY, Scripta Metallurgica, 16, (1982), 1285.

16. M. McLEAN, Acta Metallurgica, 33, (1985), 545-556.

17. A. HORSEWELL, Scripta Metallurgica, 13 (1979) 21-25.

18. E. ARZT, M.F. ASHBY, and R.A. VERRALL, Acta Metallurgica, 31, (1983), 1977-1989.

19. J.B. BILDE-SØRENSEN, Deformation of Multi-Phase and Particle Containing Materials, 4th RISØ International Symposium, eds. J.B. Bilde-Sorensen, et.al., RISØ National Laboratory, (1983), 1-14.

20. S.J. CLEGG AND J.W. MARTIN, Metal Science 16 (1982) 61-72. 21.B.

21. KASHYAP AND A.K. MUKHERJEE, Res Mechanica 17, (1986) 293-355.

22. T.R. BIELER, Ph.D. Dissertation, U.C. Davis, June, 1989.

23. M. SUERY and A.K. MUKHERJEE, Creep Behavior of Crystalline Solids, eds. B. Wilshire, R.W. Evans, Pineridge Press, Swansea, U.K. (1984), 172-192.

24. T.E. HOWSON, J.E. STULGA, D.A. MERVYN, and J.K. TIEN, Metallurgical Transactions, 11A, (1980), 1599-1616.

25. A.H. CLAUER AND N. HANSEN, Acta Metallurgica, 32, (1984), 269.

26. R.W. LUND and W.D. NIX, Acta Metallurgica, 24, (1976), 467.

27. M. OTSUKA, Y. ABE, and R. HORIUCHI, Creep and Fracture of Engineering Materials and Structures, eds. B. Wilshire, R.W. Evans, Proceedings of 3rd International Conference in Swansea, April 1987, The Institute of Metals, London, (1987), 307-317.

28. T.R. BIELER, T.G. NIEH, J. WADSWORTH, and A.K. MUKHERJEE, Scripta Metallurgica, 22, (1988), 81.

29. J.K. GREGORY, J.C. GIBELING AND W.D. NIX, Metallurgical Transactions, 16A, (1985), 777.

30. F.A. MOHAMED, Journal Material Sciences 18, (1983) 582-592.

31. Smithells Metals Reference Book, 6th ed., ed. E.A. Brandes, Butterworths, London, (1983), Chapter 13.

32. F.A. MOHAMED and T.G. LANGDON, Acta Metallurgica, 22, (1974), 779-788.

33. Diffusion and Defect Data, ed. F.H. Woehlbier, Trans Tech Publications, Switzerland, 44-45, (1986), 133, and 47, (1986), 6-7.

34. W. BLUM and B. REPPICH, Creep Behaviour of Crystalline Solids, eds. B Wilshire and R.W Evans, Pineridge Press Ltd., Swansea, U.K., (1985), 100-106.

35. R. LAGNEBORG, Scripta Metallurgica, 7, (1973), 605.

36. E. ARZT, J. ROESLER and J.H. SCHROEDER, Creep and Fracture of Engineering Materials and Structures, eds. B. Wilshire and R.W. Evans, The Institute of Metals, London, (1987), 217-230.

37. B.A. ASH and C.H. HAMILTON, Scripta Metallurgica, 22, (1988), 277-282.

38. P.R. HOWELL and G.L. DUNLOP, Creep and Fracture of Engineering Materials and Structures, eds. B. Wilshire, D.R.J. Owen, Pineridge Press, Swansea, U.K., (1981), 127-140.

39. J.E. HARRIS, Metal Science J., 7, (1973), 1-6.

40. H.J. KLAM, H, HAHN, and H. GLEITER, Acta Metallurgica, 35, (1987), 2101-4.

41. A. BALL and M.M. HUTCHINSON, Metal Science J., 3, (1969), 1-7.

42. A.K. MUKHERJEE, Materials Science & Engineering, 8, (1971), 83-89.

43. A.K. MUKHERJEE, Grain Boundaries in Engineering Materials, ed. J.L. Walter et al., Claitor Publishing, Baton Rouge, LA, (1975), 93-105.

44. H. LUTHY, R.A. WHITE and O.D. SHERBY, Materials Science & Engineering, 39, (1979), 211.

45. A.H. COTTRELL and M.A. JASWON, Proceedings of the Royal Society A, 199, (1949), 104.

46. H.W. KING, J. Materials Science, 1, (1966), 79.

47. J. FREIDEL, Dislocations, Pergamon Press, Oxford, (1964).

48. J. WEERTMAN and J.R. WEERTMAN, Constitutive Relations and Their Physical Basis, 8th RISØ, eds. S.I. Andersen, J.B. Bilde-Sorensen, N. Hansen, T. Leffers, H. Lilholt, O.B. Pedersen, B. Ralph, RISØ National Laboratory, (1987), 191-203.

49. H.J. FROST and M.F. ASHBY, Deformation Mechanism Maps, Pergamon, Oxford, (1982), 21.

TABLES

TABLE 1: COMPOSITION OF IN9021 AND IN90211

	Mg	Cu	C	O	Al_2Cu	Al_4C_3	Al_2O_3	Al
IN9021: wt%	1.5	4.0	1.1	0.8				
IN90211: wt%	2.0	4.4	1.1	0.8				91.7
* wt%	2.0	0.9			6.4	4.3	1.7	84.7
* Vol%					4.1	4.1	1.2	90.6

* Assuming 80% of Cu in Al_2Cu, O and C in Al_4C_3, Al_2O_3, and Mg in solution

TABLE 2: TENSILE TEST DATA FOR IN90211

Temp °C	True $\dot{\varepsilon}$	True UTS True	ε	MPa	True Peak True	ε	MPa	35% Elongation ε=0.30	$\dot{\varepsilon}$	65% ε=0.50	$\dot{\varepsilon}$
425	.000103	.038		25.7	.051		26.0				
425	.00105	.054		27.3	.072		27.7				
425	.0106	.050		28.8	.10		29.3	25.2	.0106		
425	.103	.048		34.1	.27		36.5	35.9	.103	35.0	.103
425	.999	.013		52.1	.25		59.2	58.2	.999	56.9	.999
425	5.15 (4.5)	.031		84.4	.135		91.3	89	4.1	81	3.3
425	25.7 (24.5)	.08		136	.12		149	142	20.6	120	16.8
425	74.7 (70.3)	.063		163	.123		179	167	59	138	48
425	316 (287) *	.05		210	.1		200				
438	1.03 (1.3)	.014		53.5	.248		58.6	56	1.43	54	1.64
438	25.5 (24.5)	.094		119	.13		136	130	20.8	114	17.1
450	.0103	.033		19.8	.082		20.1	14.8	.0103		
450	1.016	.035		37.3	.40		40.3	39	1.016	38	1.016
450	25.7 (24.6)	.105		106	.153		120	115	21.0	99	17.2
445	327 (297) *	.05		200	.1		190				
462	1.036	.056		33.2	.28		35.8	35.1	1.036	34	1.036
462	26.7 (24.8)	.07		93	.15		100	96	22.0	80	19.0
475	.000101	.07		13.3	.10		13.4	11.8	.000101		
475	.0108	.057		15.4	.083		15.5	11.2	.0108		
475	.0992	.040		16.6	.27		17.6	17.2	.0992	14.6	.0992
475	.987	.12		29.7	.28		32.0	31.8	.987	31.0	.987
475	2.5 (2.2)	.01		38.0	.215		41.5	41	2.0	38	1.7
475	9.3 (9.2)	.01		53.0	.02		53.6	48	6.9	42	5.7
475	24.2 (21.3)	.09		81	.21		85.8	83	19.6	74	16
475	74 (66)	.05		114	.165		116	114	58	97	47
475	329 (299) *	.05		167	.1		160				

Numbers in ( ) are true strain rates at peak true stress for constant displacement rate experiments.

* Accurate to 10%, otherwise values are accurate to 1%.

TABLE 3: SECONDARY CREEP RATES OF IN9021

Temp °C	ΔT	Stress MPa	$\dot{\varepsilon}$ 1/sec
475	3	10.2	4×10^{-9}
469	12	11.8	1.3×10^{-8}
475	3	13.85	1.83×10^{-7}
475	3	14.9	4.46×10^{-7}
475	4	15.8	9.99×10^{-7}
475	1	17.8	1.34×10^{-5}
475	1	19.8	2.43×10^{-4}
465	10	22.0	5.55×10^{-3}
Δσ Experiments:			
475		20.95	3.36×10^{-3}
475		17.08	$<1.4 \times 10^{-5}$
475		20.95	3.43×10^{-3}
475	1	17.0	4.88×10^{-6}
475	1	20.1	$>1.11 \times 10^{-4}$
475	1	17.0	4.56×10^{-6}

Temp °C	ΔT	Stress MPa		$\dot{\varepsilon}$ 1/sec
UTS from Initial Strain in Load Relaxation Experiments:				
475	1	22.45		0.095
475	3	36.0		0.90
ΔT Experiment:				
423	1	17.0		3.0×10^{-9}
431	1	17.0		4.2×10^{-9}
446	1	17.0		1.9×10^{-8}
435	1	17.0		2.74×10^{-9}
441	1	17.0		5.0×10^{-8}
455	1	17.0	*	7.45×10^{-7}
467	1	17.0	*	7.7×10^{-5}
485	1	17.0	*	$<5 \times 10^{-5}$

ΔT is the temperature gradient along the specimen axis.
* Was unloaded, relaxed, and changed temperature to next value. The last strain rate was measured during tertiary creep, from three datum points prior to catastrophic failure, hence creep rate at 485°C is less than the tertiary value obtained.

Hydraulic instability in testing machine caused termination of Δσ experiments prior to specimen failure.

TABLE 4: X-RAY DIFFRACTION OF IN90211

(hkl)	Al *		IN90211 Undeformed			IN90211 Deformed **		
	d (nm)	I/I_0	d (nm)	I/I_0	I/I_{Al}	d (nm)	I/I_0	I/I_{Al}
(111)	.2338	1.0	.2331	1.0	1.0	.2333	.96	.96
(200)	.2024	.47	.2020	.61	1.3	.2021	1.0	2.1
(220)	.1431	.22	.1430	.29	1.3	.1431	.31	1.4
(311)	.1221	.24	.1220	.34	1.4	.1221	.47	2.0
(222)	.1169	.07	.1168	.08	1.1	.1169	.11	1.6

* Joint Committee on Powder Diffraction Standards, card number 4-787
** 2.5/sec, 475°C

TABLE 5: MEASURED AND EXTRAPOLATED THRESHOLD STRESSES

	425	438	450	462	475	492 °C
IN9021l: Tensile Modified Average Extrapolation						
n=3	16	10.2	6.8	4.7	3.2	1.9
n=2	33	28	23	19	16	13
IN9021l: Load Relaxation	9±2					
IN9021: Load Relaxation					<7	4.7±1.4
IN9021: Otsuka Method (n=2)					17	

All stresses are tensile, σ, where $\sigma = \tau\sqrt{3}$

TABLE 6: ACTIVATION ENERGIES FOR IN90211

Method of Measure	(kJ/mol)	
$Ln(\dot{\varepsilon}T/G) - nLn((\sigma_a-\sigma_i)/G)$:	n=2	n=3
Peak Load (UTS)	79	103
Peak True Stress	98	119
True $\sigma(\varepsilon=0.3)$	105	124
True $\sigma(\varepsilon=0.5)$	96	133
Average:	95±10	120±17
Ln(Threshold Stress): (n)	60±10	140±5

Values of diffusivity used for plots:

	D_o, m^2/sec	Q, kJ/mol
Al self diffusion [1]	225×10^{-6}	145
Mg in Al/2.2at%Mg [2]	21×10^{-6}	128
Chemical, Al/2.2at%Mg [3]	1200×10^{-6}	143
Chemical, Al/0-2%Cu [4]	18×10^{-6}	126
Al Grain boundary diffusion *	10^{-14}	60

* The frequency term for grain boundary diffusion contains the width of grain boundary, $\delta \approx$ 2-3 times the Burgers vector [5].

1. M. BEYELER, These-Paris; J. Physics (Fr.), 29, (1968) 345.
2. STOEBE, et al., Acta Metallurgica, 13, (1965), 701.
3. H. BUCKLE, Z. Electrochem., 49, (1943), 238.
4. J.R. CAHOON, Metallurgical Transactions, 3, (1972), 1324.
5. H.J. FROST and M.F. ASHBY, Deformation Mechanism Maps, Pergamon, Oxford, (1982), 21.

FIGURES

Fig 1. a) elongation and b) applied true stress as a function of true strain rate for tensile experiments on IN90211.

Fig 2. A family of true stress-strain curves at 475°C and various strain rates.

Fig 3. Comparison of tensile and creep data for IN90211 and IN9201.

Fig 4. Stress change experiment of IN9021 showing inverted transients.

Fig 5. Extrapolations of the linearized stress-strain rate data to zero strain assuming n=2, 3, and 4, where n=1/m, show temperature dependent threshold stresses.

Fig 6. Extrapolated threshold stresses increase slightly with strain. Average values are indicated on the vertical axis.

Fig 7. The apparent activation energy depends upon the stress.

Fig 8. The true activation energy at the UTS (based upon n=2 and n=3 assumptions).

Fig 9. The activation energy of the threshold stress, showing the effect of strain.

Fig 10. General and local climb describe different paths for dislocation lines overcoming particles.

Fig 11. The effect of threshold stresses arising from general and local climb on the stress-strain rate behavior is compared.

Fig 12. Mixed climb for Threshold stresses a) 0.5 times Orowan stress (ϕ=30°), and b) 0.1 times Orowan stress (ϕ=6°).

Fig 13. Normalized plots of IN90211 superplastic data with respect to a) grain boundary diffusion, b) Mg diffusion in Al, and c) lattice self diffusion in Al. Deformation models are plotted for comparison.

Fig 14. Normalized plots of IN90211 superplastic data with respect to a) grain boundary diffusion, b) Mg diffusion in Al, and c) lattice self diffusion in Al. Deformation models are plotted for comparison.

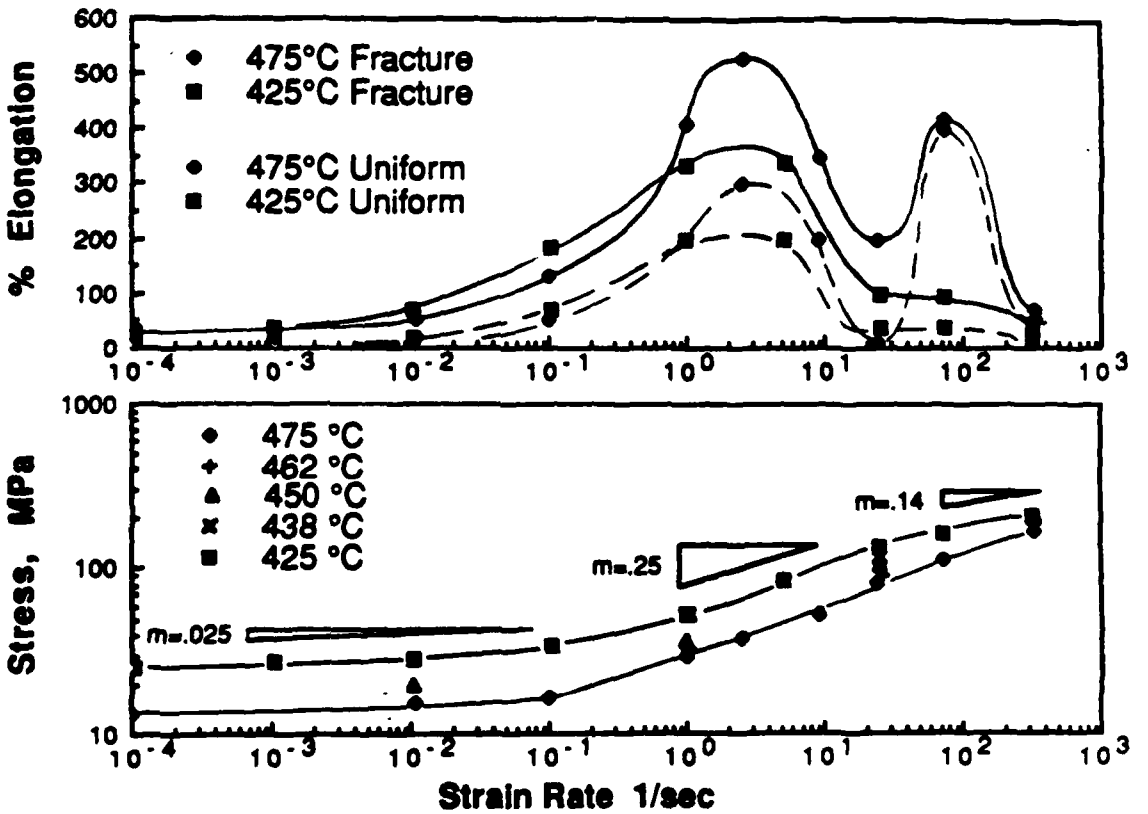
% Elongation
600
500
400
300
200
100
0
475°C Fracture
425°C Fracture
475°C Uniform
425°C Uniform
Stress, MPa
1000
100
10
475 °C
462 °C
450 °C
438 °C
425 °C
m=.025
m=.25
m=.14
10⁻⁴
10⁻³
10⁻²
10⁻¹
10⁰
10¹
10²
10³
Strain Rate 1/sec

Fig. 1

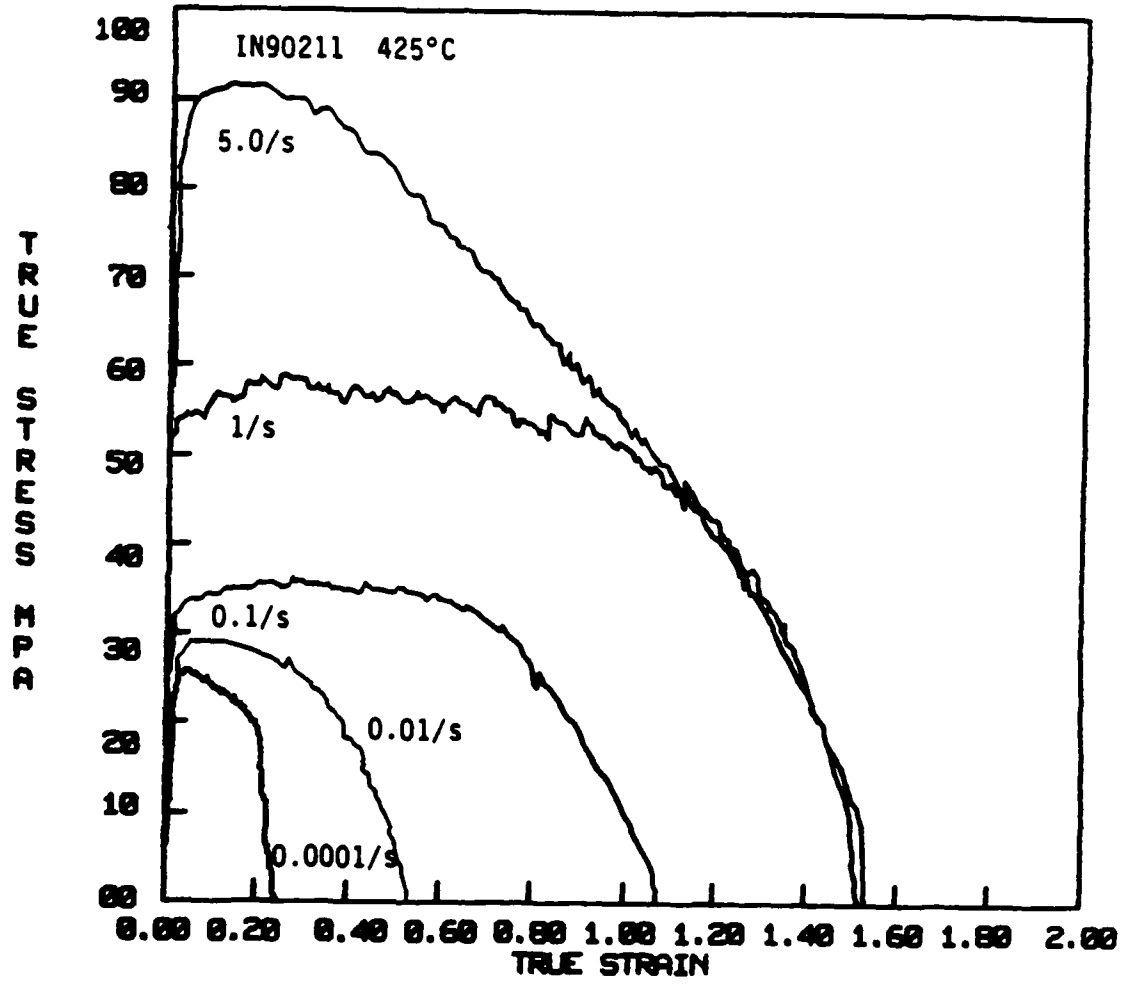
IN90211 425°C
5.0/s
1/s
0.1/s
0.01/s
0.0001/s
TRUE STRESS MPA
100
90
80
70
60
50
40
30
20
10
00
0.00 0.20 0.40 0.60 0.80 1.00 1.20 1.40 1.60 1.80 2.00
TRUE STRAIN

Fig. 2

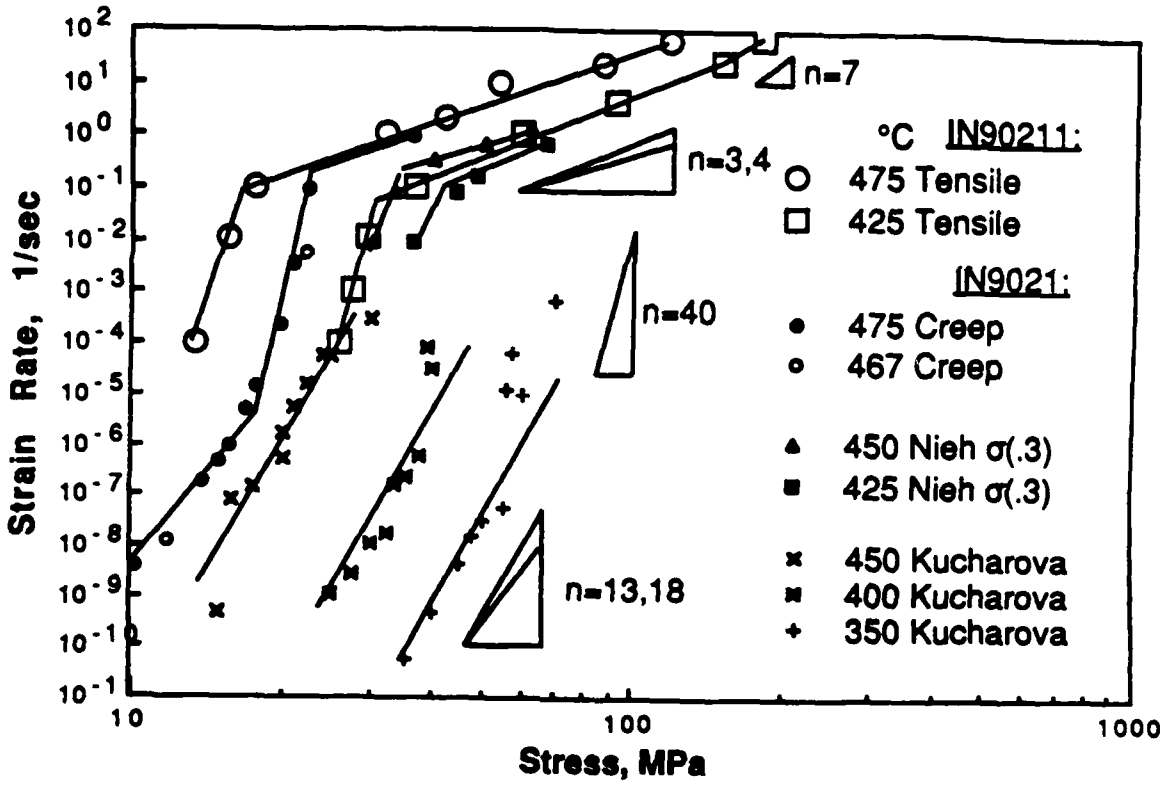
Strain Rate, 1/sec
Stress, MPa
n=7
n=3,4
n=40
n=13,18
°C IN9021:
475 Tensile
425 Tensile
IN9021:
475 Creep
467 Creep
450 Nieh σ(.3)
425 Nieh σ(.3)
450 Kucharova
400 Kucharova
350 Kucharova

Fig. 3

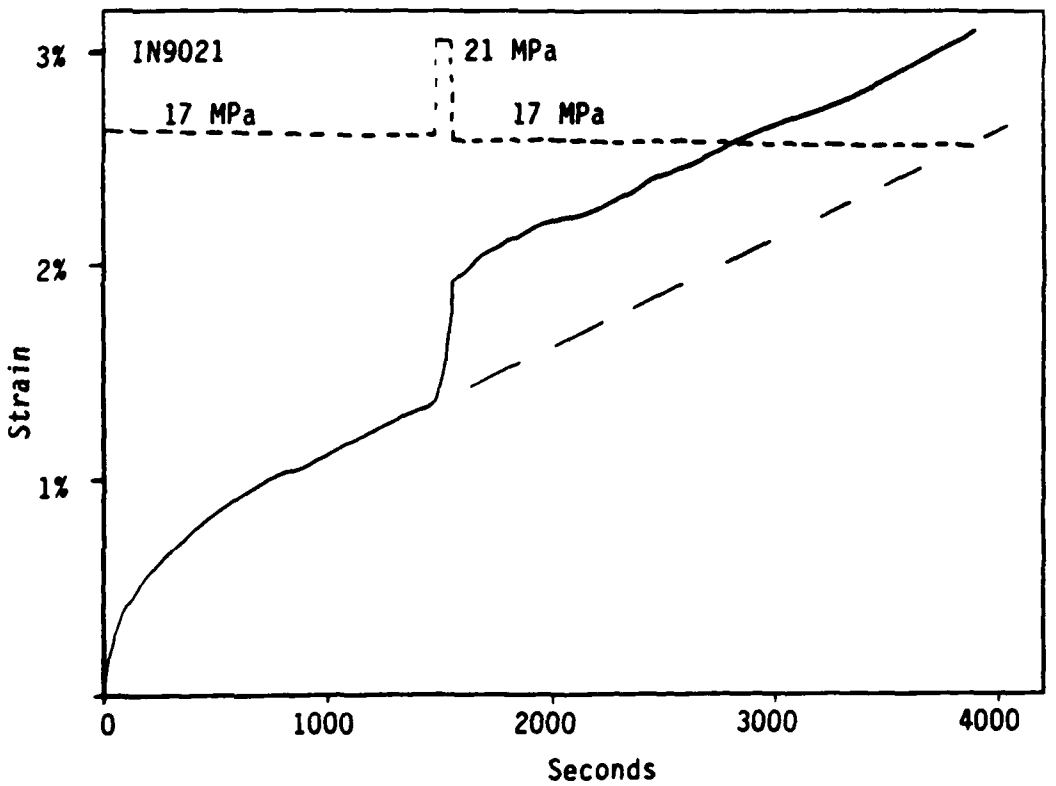
IN9021
17 MPa
21 MPa
17 MPa
Strain
Seconds

Fig. 4

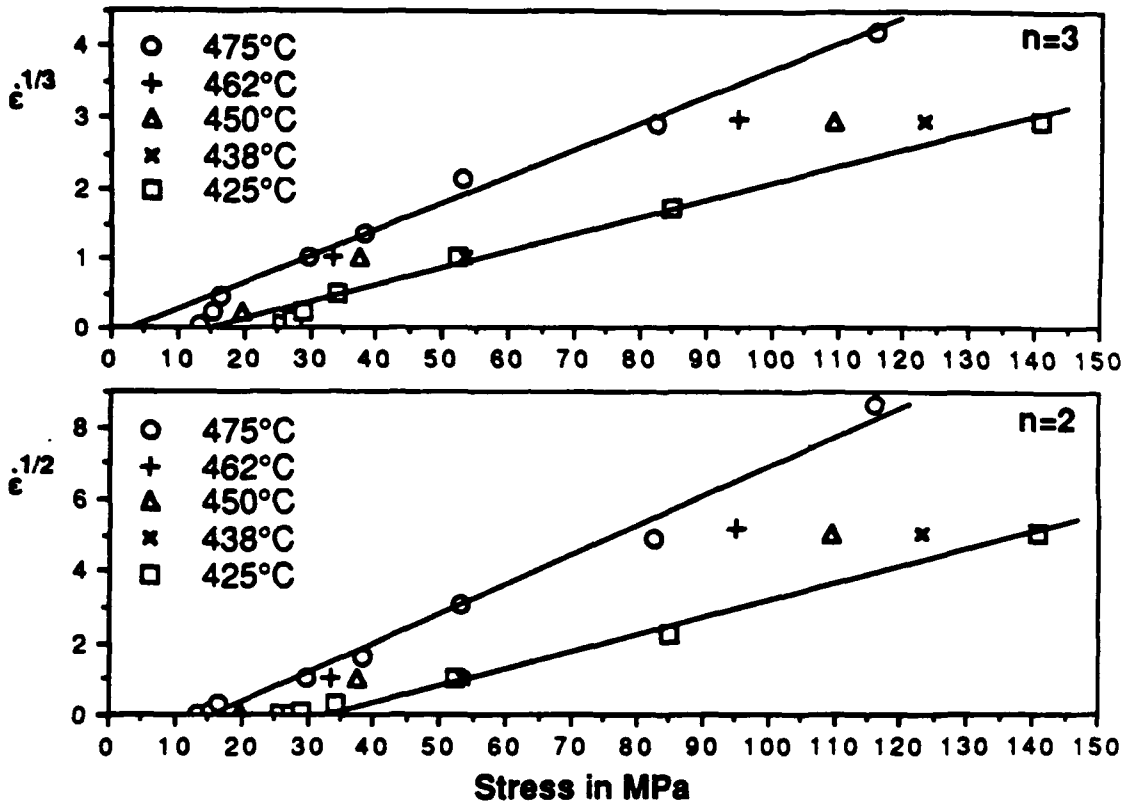
n=3
475°C
462°C
450°C
438°C
425°C
$\dot{\varepsilon}^{1/3}$
n=2
$\dot{\varepsilon}^{1/2}$
Stress in MPa

Fig. 5

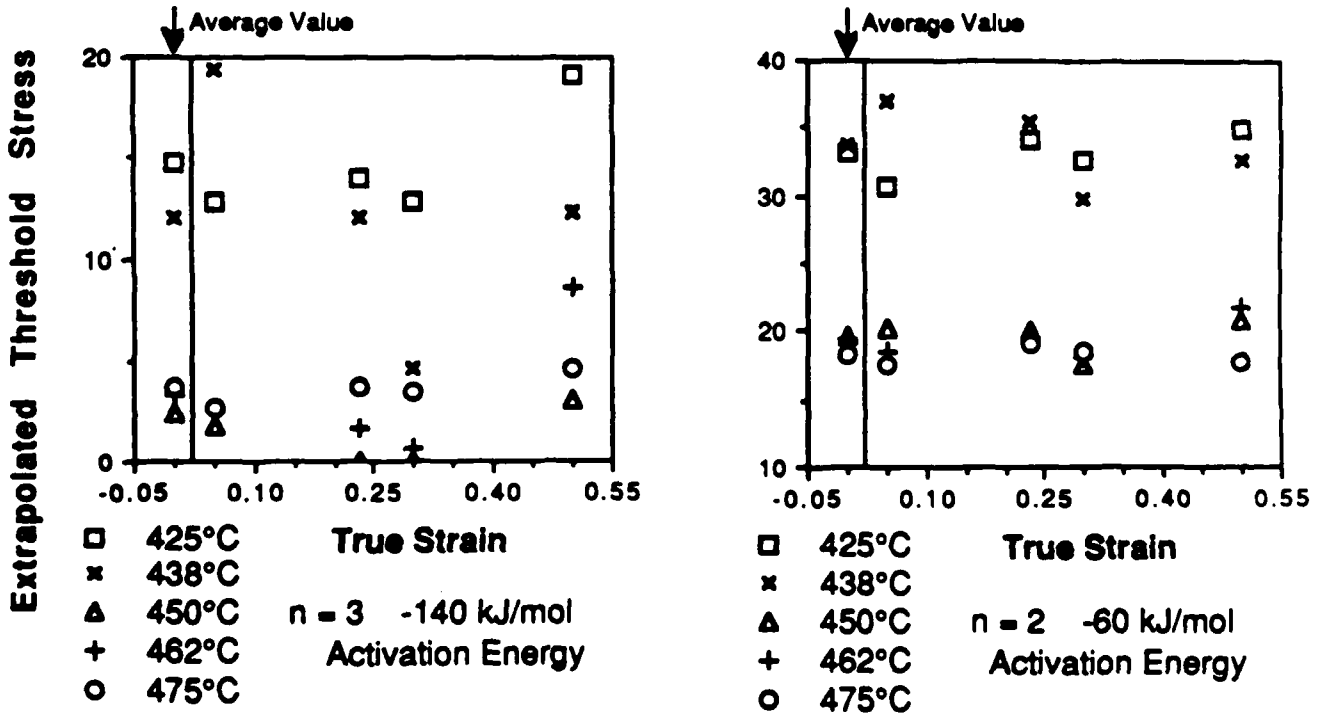
Average Value
Extrapolated Threshold Stress
True Strain
425°C
438°C
450°C
462°C
475°C
n = 3 -140 kJ/mol
Activation Energy
n = 2 -60 kJ/mol

Fig. 6

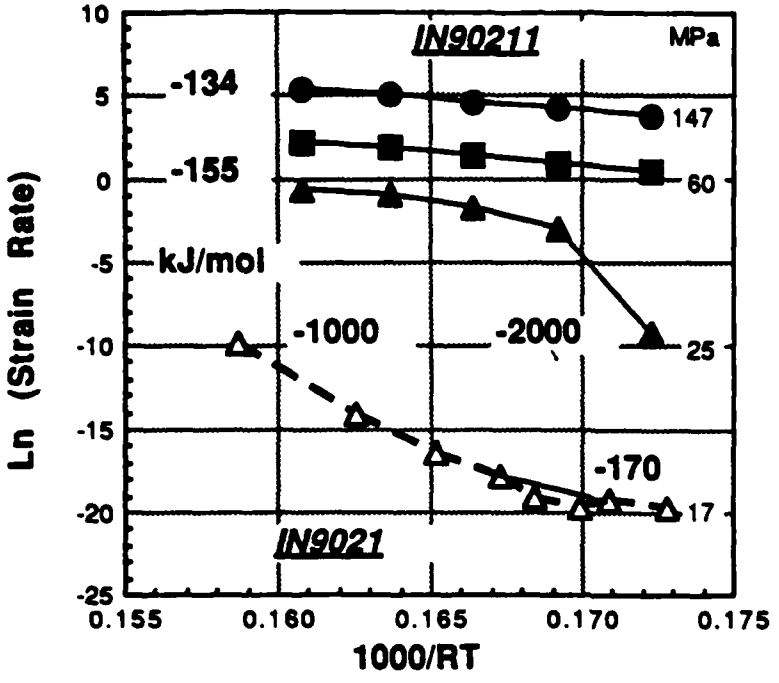

Fig. 7

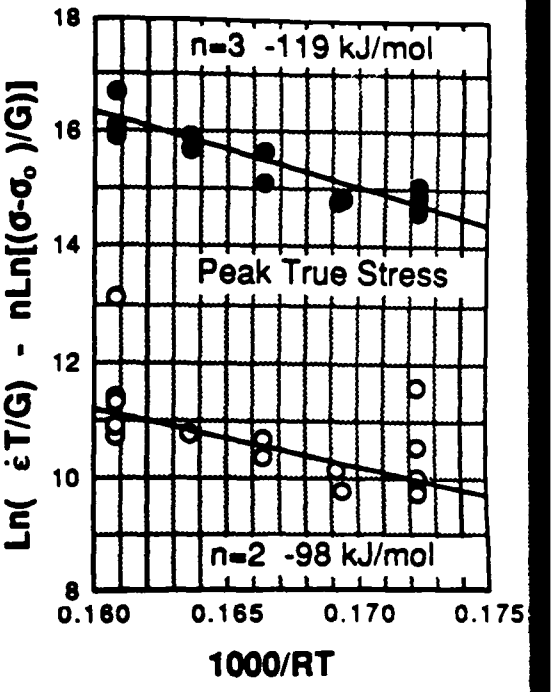

Fig. 8

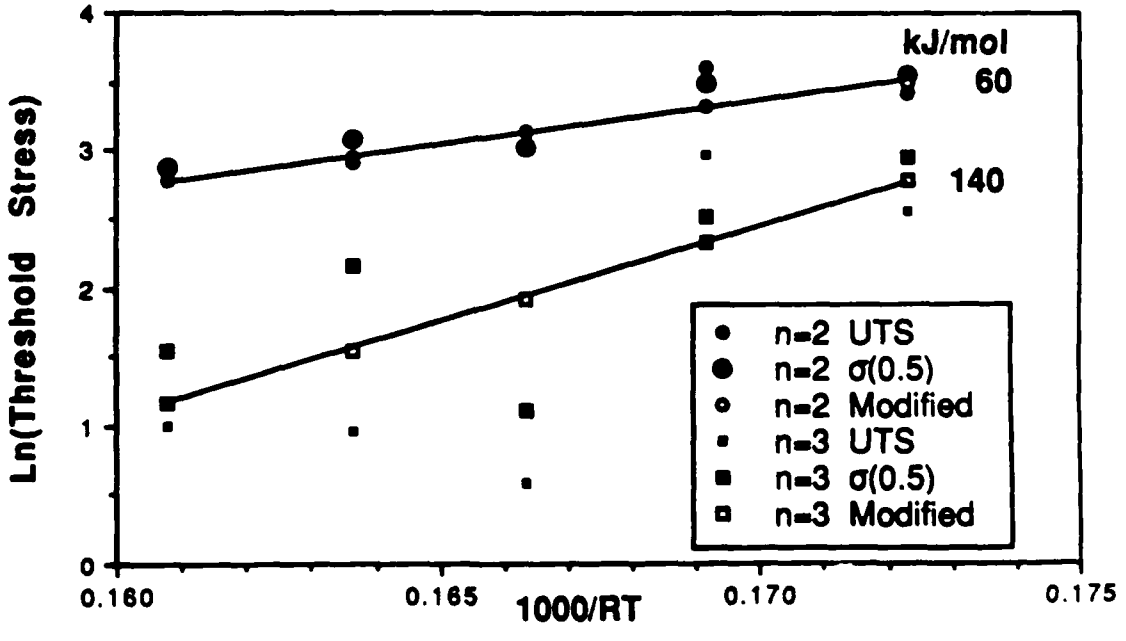

Fig. 9

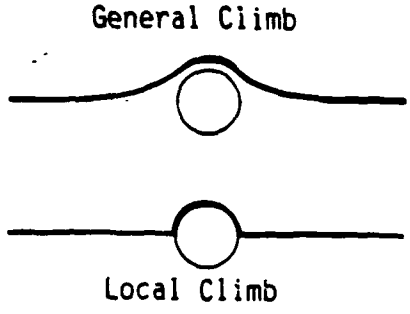

Fig. 10

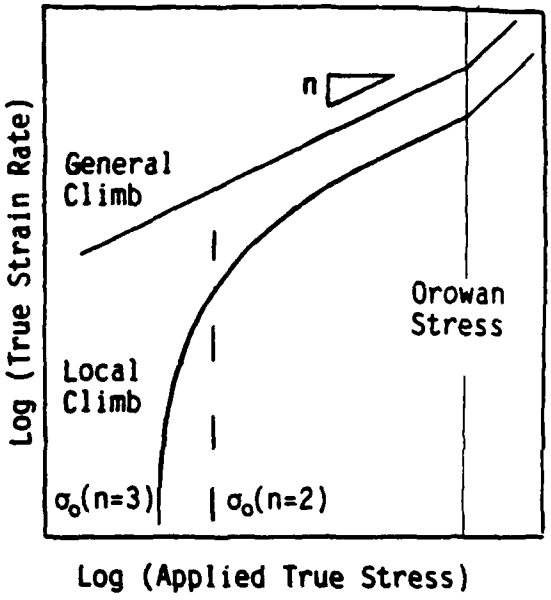

Fig. 11

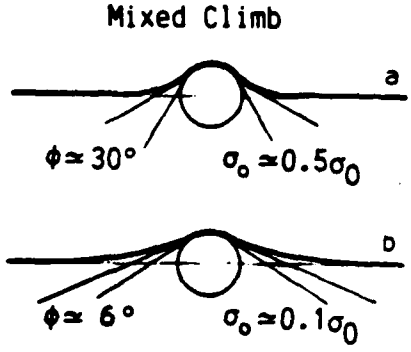

Fig. 12

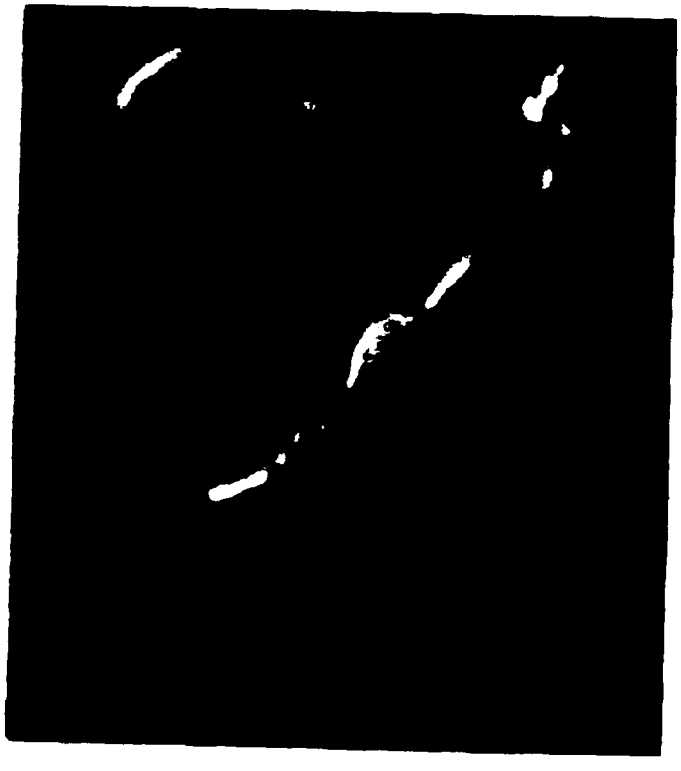

Fig. 13 20nm

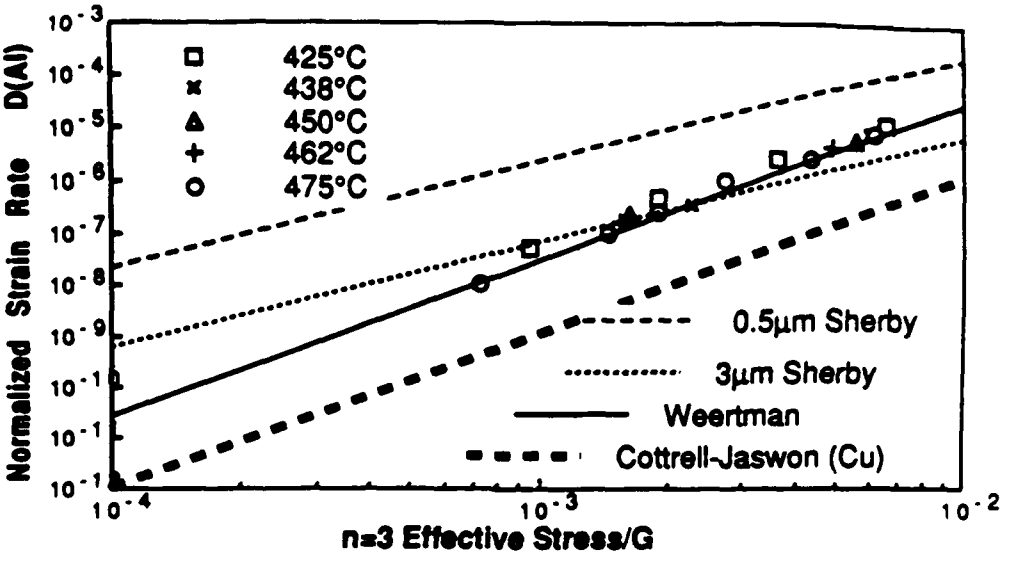
Normalized Strain Rate D(Al)
425°C
438°C
450°C
462°C
475°C
0.5μm Sherby
3μm Sherby
Weertman
Cottrell-Jaswon (Cu)
n=3 Effective Stress/G

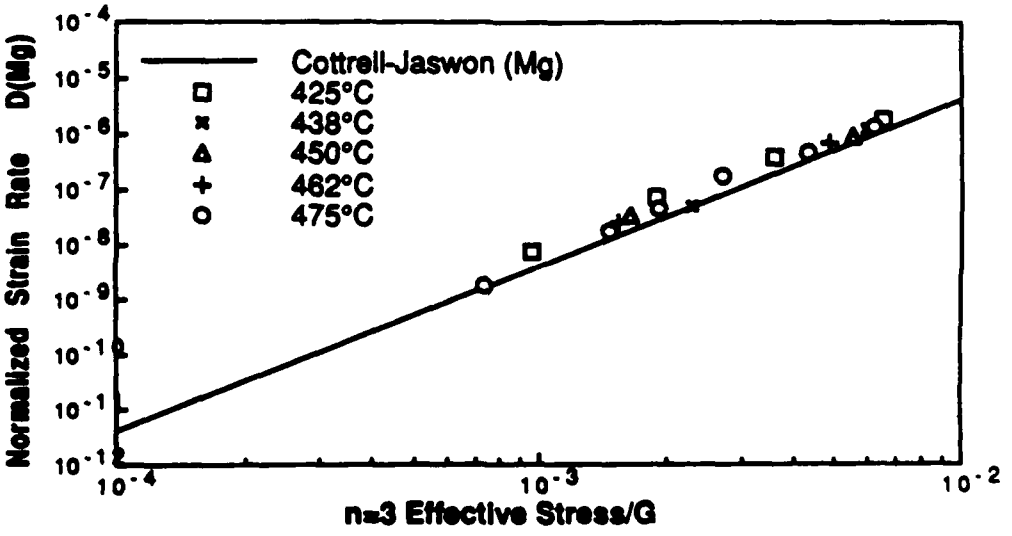
Normalized Strain Rate D(Mg)
Cottrell-Jaswon (Mg)
425°C
438°C
450°C
462°C
475°C
n=3 Effective Stress/G

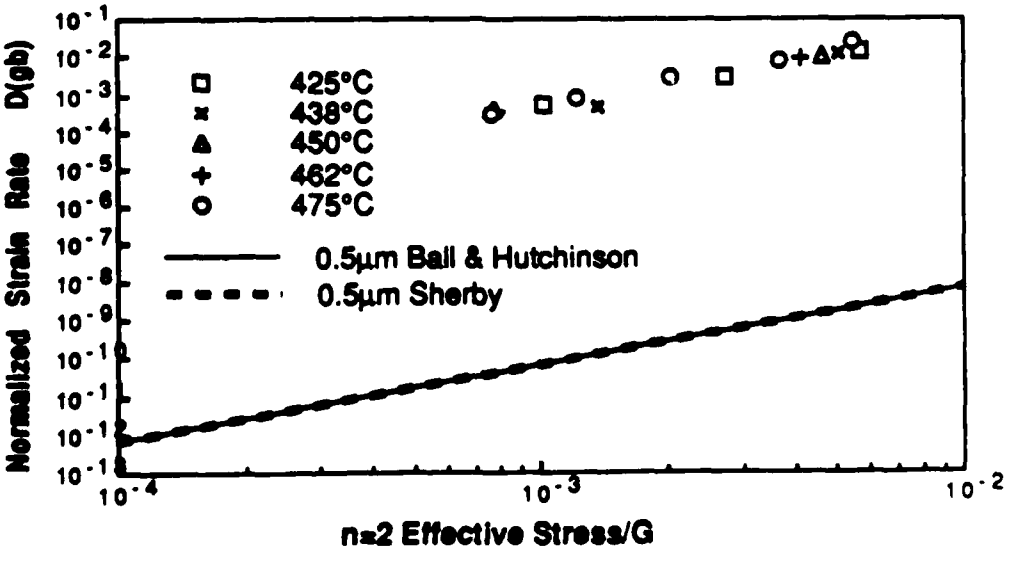
Normalized Strain Rate D(gb)
425°C
438°C
450°C
462°C
475°C
0.5μm Ball & Hutchinson
0.5μm Sherby
n=2 Effective Stress/G

Fig. 14

II. THE ROLE OF ADIABATIC HEATING ON HIGH RATE SUPERPLASTIC ELONGATION

Superplasticity has been growing in its applicability for cost effective forming of parts. The major economic consideration for its use has been that the forming process has required times on the order of an hour or more to form a part. Recent work with an extremely fine grained aluminum alloy has shown that superplasticity is possible at strain rates on the order of 1-10/sec, where 500% elongation was obtained in a few seconds [1]. It is well established that adiabatic heating, a condition encountered at high strain rates, can affect the temperature of the deforming material, leading to thermal instabilities that can lead to catastrophic failure. The effect of adiabatic heating can cause premature fracture of a superplastically deforming material, but it can be used beneficially if the strain rate is changed appropriately.

Superplasticity is a subset of creep behavior that describes the reverse of the usual goal of creep-resistance. The following conditions have been necessary, though not sufficient for obtaining superplastic deformation in practical time-scales: high temperature (greater than half the absolute melt temperature); a stable, equiaxed, fine grain size, (usually $< 10\ \mu m$); minimal cavitation in order to prevent premature fracture, and a strain rate sensitivity parameter m greater than 0.3 and/or a positive strain hardening exponent h that promotes neck stability. The latter condition will be addressed in this paper. A constitutive equation commonly used to describe superplasticity, based upon the true strain, ϵ, the strain rate exponent, m, the strain hardening exponent h, and the strain hardening parameter γ, is

$$\sigma = K\dot{\varepsilon}^{m}\varepsilon^{h}; \quad m = \left(\frac{\partial \ln \sigma}{\partial \ln \dot{\varepsilon}}\right)_{\varepsilon}, \qquad h = \gamma\varepsilon = \left(\frac{\partial \ln \sigma}{\partial \ln \varepsilon}\right)_{\dot{\varepsilon}} = \frac{\varepsilon}{\sigma}\left(\frac{\partial \sigma}{\partial \varepsilon}\right)_{\dot{\varepsilon}} \qquad (1)$$

where K is a constant based upon microstructural details. The deformation of superplastic metals and alloys usually exhibits a sigmoidal curve on a logarithmic plot of stress and strain rate, where maximum elongations occur where m is maximum.

Flow stability of deformation has recently been reviewed by Nichols [2]. The final fracture elongation can be integrated from flow stability relations based upon m and γ values assuming that the strain at fracture approaches infinity. With a geometric perturbation defined by $f = \delta A/A$ (regardless of how such an imperfection arises), final fracture strains can be predicted in the form $\varepsilon = f(m,f,\gamma)$ [2]. Such analytical expressions predict the correlation given by Woodford [3] relating the m value with total elongation. The scatter of the data suggest that f falls between 0.1 and 0.001 in the various theories, which corresponds to nearly an order of magnitude in elongation. These results demonstrate the strong dependence of elongation upon m and f.

The parameter f, describing an inhomogeneity in geometric shape of the specimen, can also be used to quantify the effects of microstructural and thermal inhomogeneities. Processing procedures can introduce variations in the microstructure that affect flow characteristics. An inclusion or a void is a flaw that can have a similar effect as a geometrical defect. Thermal gradients can be related to geometric inhomogeneities to determine the temperature stability required for flow stability. Given the strong thermal dependence of equation (1), a thermal inhomogeneity can be defined by [4].

$$f_T = 1-\exp[m(1-Q/RT)\Delta T/T]. \quad (2)$$

A thermal inhomogeneity of 3°C can reduce potential elongation by a factor of 2 in aluminum alloys.

A. EXPERIMENTAL PROCEDURE AND RESULTS

Tensile specimens were made from processed IN90211 sheet material produced by Novamet, Inc. (lot 85V032), and subsequently processed at the Research and Development Labs of Lockheed Missiles and Space Company. The extruded rod was forge flattened and warm rolled to sheet 2.5 mm thick, annealed and water quenched. Specimens had a gage length of 6.3 mm, and were nominally 2.5 mm square. Specimens were marked with pencil, and photographed before and after deformation, to permit accurate local strain and area reduction measurements. Deformation took place at 425-475 °C in a computer controlled hydraulic testing machine. Specimens were tested at constant true strain rate up to 1/sec strain rate, and at constant displacement rate at higher rates. The specimens were heated in a radiant furnace, and deformed within 10 minutes of reaching a stable temperature. The temperature differential between the two ends was kept within 3°C. A 5°C increase was typically monitored at the shoulders of the specimens following deformation at the higher strain rates. The results of the experiments were typical for superplasticity, exhibiting three deformation regimes (Fig. 1), with maximum elongations occurring where the strain rate sensitivity is highest in the middle regime. The dip in the elongation curve in the middle of the superplastic regime is intriguing and the reason for its presence is addressed below.

For specimens showing high elongations, the true stress-strain curves typically exhibit an extensive stress plateau region (Fig. 2), indicating a uniform elongation prior to necking. Slight strain softening was observed, increasing in magnitude with decreasing temperature. A plateau was not seen in specimens deformed under constant displacement rate, since the true strain rate decreased with strain. One experiment was conducted to determine flow behavior under increasing true strain rate. This was done using the constant true strain rate program, but the displacement-time curve was determined based upon a gage length 40% shorter than the actual specimen length. This resulted in an increasing (though decelerating) true strain rate by a factor of 2, at a true strain of 1 (438°C). This flow curve did not exhibit any increase in the apparent hardening behavior. Rather, the flow curve softened even more than the specimen strained at constant true strain rate at a lower temperature (425°C).

The reduction of area as a function of specimen length is a way of illustrating the uniformity of deformation. Profiles at fracture for several specimens are shown in Fig. 3. Unlike more typical superplastic deformation, there is no well defined plateau of reduced area at fracture, which is consistent with the usual observation of a diffuse neck. (The only exception was the specimen deformed at 75/sec at 475°C, which did not have a diffuse neck.) The area reduction (R.A.) and engineering strain (ϵ) correlated for many specimens at many strain rates according to the relation between engineering strain ϵ and area reduction, $R.A. = (A_o-A)/A_o = \epsilon/(1+\epsilon)$.

B. ANALYSIS

One of the consequences of high rate deformation of metals is the generation of heat in the specimen that results from rapid strain energy dissipation. At low strain rates, conduction of heat to the ends of the specimen allows the test to remain isothermal. At extremely high deformation rates generation of heat occurs much faster than it can be conducted to the ends of the specimen (acting as heat sinks). In the absence of conduction, it can be assumed that all of the adiabatically heat generated will raise the temperature of the specimen. This can be estimated with the following equation, which converts the dissipated strain energy into an increase in temperature:

$$\Delta T = \frac{B\ w}{C_p \rho} \int \sigma d\varepsilon \qquad (3)$$

$\Delta T = B(0.33\ m^3/MJ)(\int \sigma d\varepsilon)$ for aluminum between 400 and 500 °C, where σ is the true stress, ε the true strain, ρ the density, w the atomic weight, and C_p is the heat capacity [5]. B is a function of strain rate, thermoconductivity, heat transfer coefficients, and specimen geometry, that is between 0 and 1, such that B=0 for isothermal conditions (usually $<10^{-3}$/sec), and B=1 for adiabatic conditions (usually > 1/sec, [6]).

The major factor affecting the value of B is the relationship between specimen geometry and the thermal conductivity of the specimen. The thermal conductivity of the aluminum alloys is 150 W/m/°C, where thermal diffusivity D_T is 5×10^{-5} m^2/s [5]. The response of the adiabatically heated (to temperature $T_\circ$) deformed part of the specimen of length $l_\circ+\Delta l$ to a constant temperature of T_∞ at both ends can be estimated from the

solution of an infinite plate heat source with the origin at the center of the specimen [7]. Assuming $l_o \approx 0.0065$ m, and 100% elongation, the problem can be solved for several times, and is shown in Fig. 4. This figure indicates that the variation in B from 0 to 1 will occur for deformation that occurs between .01 and 10 seconds for the geometry of the specimen used. The transition from isothermal to adiabatic conditions (indicated by the value of B) occurs at strain rates between 1 and 50/sec (Fig. 1c). The geometry of the actual specimen would be more effective as a heat sink than this linear estimate, due to the increasing specimen area at the shoulder. Combined with the decreasing cross sectional area of the deforming region, the temperature profile in the middle would actually be more peaked than calculated. This calculation then represents a lower bound for the conductivity problem.

From the above analysis, adiabatic heating clearly occurs in the superplastic regime. Adiabatic heating affects the stress in the sample since the flow stress is a strong function of temperature (Fig. 1). Therefore a local increase in temperature will promote localized straining due to the lower flow stress, and elongation will occur preferentially in hotter regions of the specimen. In the time frame between isothermal and adiabatic heating conditions, the temperature will be smoothly peaked in the middle.

The temperature profile in the specimen can be estimated as a function of strain in a deforming specimen. From equation (3), the measured strain energy increases as a function of strain as shown in Fig. 5. Use of equation (2) permitted adiabatic temperature rise to be calculated as a function of strain. With the value of B taken from Fig. 1c, temperature profile at selected strains can be calculated, as

illustrated in Fig. 6. The increasing area at the ends of the specimen has the effect of compressing the axial dimension in the shoulder [8]. Three specimens initially at 475°C were deformed at strain rates of 2.5/sec, 25/sec, and 75 sec. The calculated temperature profiles show substantial similarity to the area reduction curves in Fig. 2. The smooth peak in the temperature profile thus makes a diffuse neck understandable solely from the considerations of the temperature distribution. Such a diffuse neck (Fig. 2) is different from that usually observed in superplastic deformation, where the reduction of area is more constant along the axial dimension. The only specimen exhibiting a constant reduction of area was the specimen deformed at 75/sec. In this specimen, the temperature variation along the tensile axis was very nearly constant, though the temperature of the deforming region was increasing uniformly with increasing strain.

Increasing or decreasing strain rate affects the elongation obtained. The greatest elongation was obtained in an experiment at constant displacement rate, rather than at constant true strain rate. At strain rates below 2/sec, the temperature profile along the specimen is quite flat, varying by less than 10%. The increasing length of the specimen accentuates the peak in the temperature as the length of the conductivity path increases. Consequently the decelerating true strain rate lowers the stress, and thus the amount of heat generated. The experiment at an increasing true strain rate had an increasing rate of heat generation due to the increasing flow stress. The increase in strain rate moved the specimen more toward the rates where adiabatic heating and conduction produces a larger thermal strain instability.

This geometry and rate effect can also help explain the smaller

elongations obtained by Nieh, et. al. [9], who used specimens twice as long. The longer conductivity path accentuates the diffuse temperature peak in longer specimens (and thus propensity for local strain enhancement). The dip in superplastic elongation was shifted to lower strain rates for longer specimens. Similarly, an elongation dip at higher strain rates could be predicted for shorter specimens. Therefore optimum elongation at high strain rates is strongly dependent upon the details of the conductivity path for heat generated adiabatically, and thus on the specific geometry of the specimen.

Flow stability theory indicates that flow stability is enhanced by a slightly positive hardening exponent. The peak true stress of the specimen deformed at 2.5/sec and 475°C was 42 MPa, but the stress based upon the final area (98.8% R.A.), at fracture was 56 MPa, which was at a much higher, but unknown temperature. Although the apparent strain hardening exponent is negative, due to adiabatic heating and the geometric softening associated with the diffuse neck, the material flow hardens on a microstructural level until fracture occurs.

Flow stability increases with increasing temperature for IN9021. The specimens deformed at 1/sec at 425 and 475 °C are shown in Fig. 3, indicating a more negative slope at the lower temperature. The contribution to the temperature increase (and thus flow softening) comes from the strain energy of deformation. A greater increase in temperature causes a greater decrease in flow stress, since stress decreases exponentially with increasing temperature. The strain energy for a given strain (and thus the adiabatic temperature increase), increases with decreasing temperature. Increasing the temperature decreases the strain energy, and thus the adiabatic temperature increase

that causes the decrease in flow stress is smaller. This leads to a smaller contribution to flow softening with increasing temperature, and therefore greater elongation.

The higher temperature not only creates a smaller temperature increase, but also a smaller temperature gradient within the specimen, in the case where deformation is affected by conduction of adiabatically generated heat. In this case the driving force for localized deformation is smaller, thereby prolonging uniform strain. These two effects, of less flow softening, and less flow localization at higher temperature account for the larger elongations obtained. The adiabatic flow softening contribution depends upon the actual work hardening rate, and the thermal diffusivity, and the specific specimen geometry.

The use of predictive elongation equations depends upon the m value and the inhomogeneity parameter f. The data of Fig. 1 indicate that an appropriate m value is approximately 0.25. The appropriate f value depends upon the temperature profile, as given in Fig. 7 and equation (2). The appropriate activation energy is that of lattice diffusion, with $Q \approx 145$ kJ/mol (Section I). Since machining defects ($f \approx 0.001$), and cavitation are essentially negligible (<1% in the superplastic regime [8], predictions of elongation in Table I can be made using the above parameters [2]. The perfectly plastic criteria underestimates the elongation, and the Duncombe criteria overestimates the elongation, but Hart's criteria is close to the observed values. These predictions are extremely sensitive to the value of m, but given opposing effects from the probably low predicted temperatures and that the m value is slightly larger than 0.25, Hart's condition best describes the superplastic elongation of IN92011. If deformation could be accomplished

isothermally, Hart's criteria would predict 1000% maximum elongation.

C. CONCLUSIONS

The elongation of high rate superplastic materials, is strongly affected by the thermal flow instability resulting from conduction of adiabatically generated heat during deformation. The dip in elongation in the middle of the superplastic regime of IN90211 is a consequence of the particular geometry of the 6.35 mm long tensile specimens used. The dip in elongation can be shifted to the right or left with smaller or longer gage lengths, respectively. Maximum elongations were obtained at the highest temperatures, since the strain energy that is converted to heat is lower than at higher temperatures. The predictions of elongations provided by Hart's flow stability criteria predict the elongation, based upon the thermal instability resulting from adiabatically generated heat.

REFERENCES

1. T.R. BIELER, T.G. NIEH, J. WADSWORTH, and A.K. MUKHERJEE, Scripta Metallurgica, 22 (1988) 81-86.

2. F.A. NICHOLS, Acta Metallurgica, 28, (1980), 663-673.

3. D.A. WOODFORD, Transactions American Society for Metals, 62, (1969), 291.

4. C.H. HAMILTON, 7th International Conference on the Strength of Metals and Alloys, eds. H.J. McQueen, et.al., Pergamon Press, Oxford, (1985), 1831-1857.

5. Smithells Metals Reference Book, 6th ed., E.A. Brandes, ed., Butterworths, London, (1983).

6. J.F. THOMAS, Jr., and R. SRINIVASAN, in Computer Simulation in Materials Science, ASM, Metals, Park, OH, (1986).

7. H.S. CARSLAW and J.C. JAEGER, Conduction of Heat in Solids, 2nd ed., Oxford Press, London, (1959), 54.

8. T.R. BIELER, Ph.D. Dissertation, University of California at Davis, 1989.

9. T.G. NIEH, P.S. GILMAN, and J. WADSWORTH, Scripta Metallurgica, 19, (1985), 1375.

TABLES AND FIGURES

TABLE I: Stability Criteria and Elongation Prediction in ε (% elongation)

Specimen: °C	$\dot{\varepsilon}$	ΔT	f_T	Perfectly Plastic $-mLn[1-(1-f)^{1/m}]$	Hart (γ-1=0) $(1/f)^m - 1$	Duncombe (γ-m-1=0) $(1/f)^{m/(1-\gamma)} - \gamma$
475	25	10	0.08	0.32 (37%)	0.9 (140%)	1.9 (550%)
475	2.5	3	0.02	0.63 (88%)	1.7 (425%)	2.6 (1300%)
Hypothetical			0.001	1.38 (300%)	4.6 (1000%)	5.5 (2500%)

Fig. 1 a) Elongation; b) Ultimate Tensile Strength as a function of strain rate; c) Adiabatic Heating Conduction Function for 6.35 mm Specimen Strained to 100% Elongation.

Fig. 2 True stress-strain curves for constant true strain rate, decreasing true strain rate, and increasing true strain rate tests.

Fig. 3 Reduction of area for several specimens shows formation of a diffuse neck.

Fig. 4 Heat conduction in deforming 6.35 mm specimen at 100% elongation under adiabatic heating conditions,

Fig. 5 Temperature increase from dissipation of strain energy into heat for several specimens.

Fig. 6 Adiabatic heating in three experiments at 475°C at different strain rates showing the effect of the large thermal gradient leading to low elongation at 25/sec.

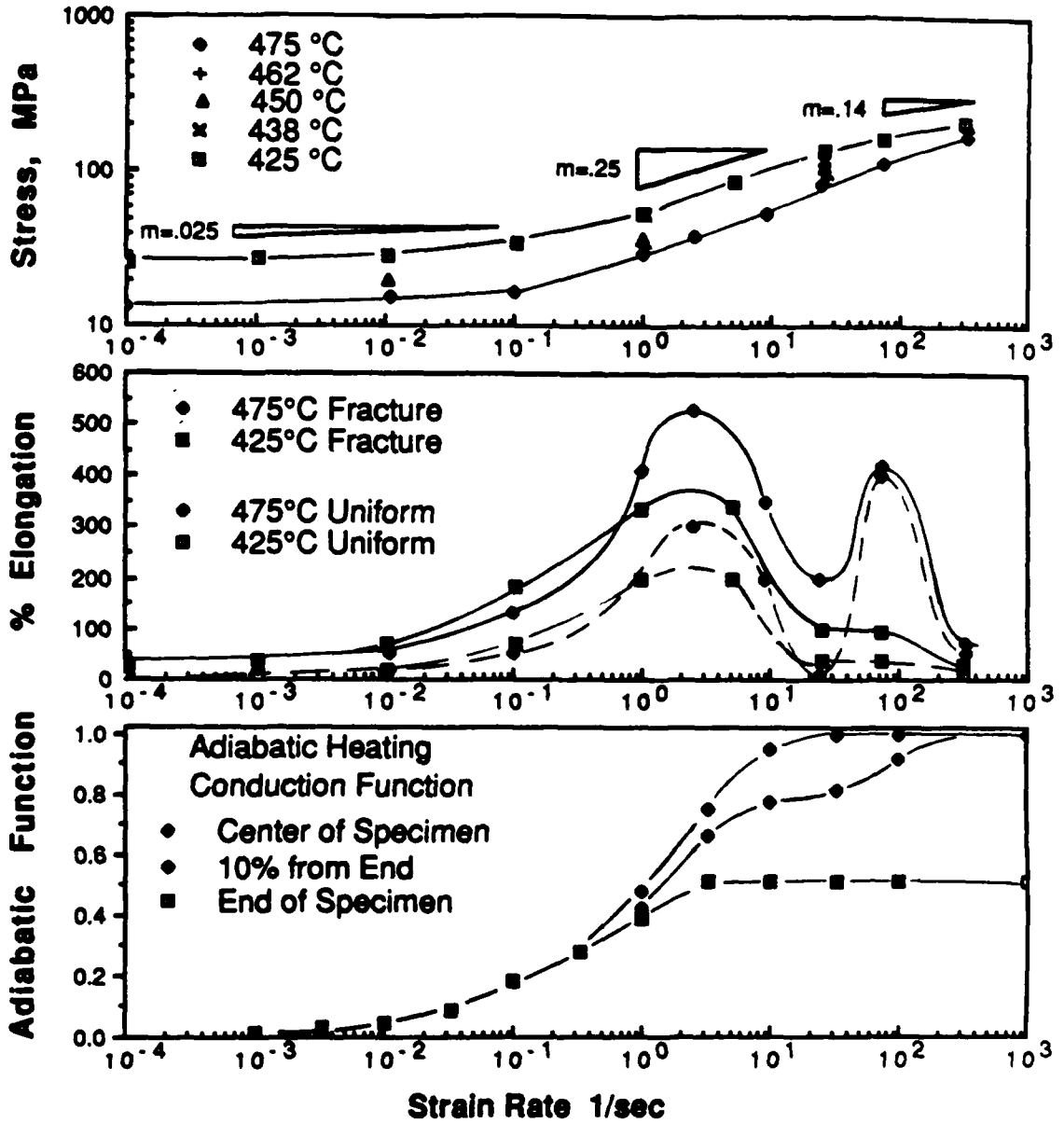
Stress, MPa
1000
100
10
475 °C
462 °C
450 °C
438 °C
425 °C
m=.025
m=.25
m=.14
% Elongation
600
500
400
300
200
100
0
475°C Fracture
425°C Fracture
475°C Uniform
425°C Uniform
Adiabatic Function
1.0
0.8
0.6
0.4
0.2
0.0
Adiabatic Heating
Conduction Function
Center of Specimen
10% from End
End of Specimen
10^{-4} 10^{-3} 10^{-2} 10^{-1} 10^{0} 10^{1} 10^{2} 10^{3}
Strain Rate 1/sec

Fig. 1

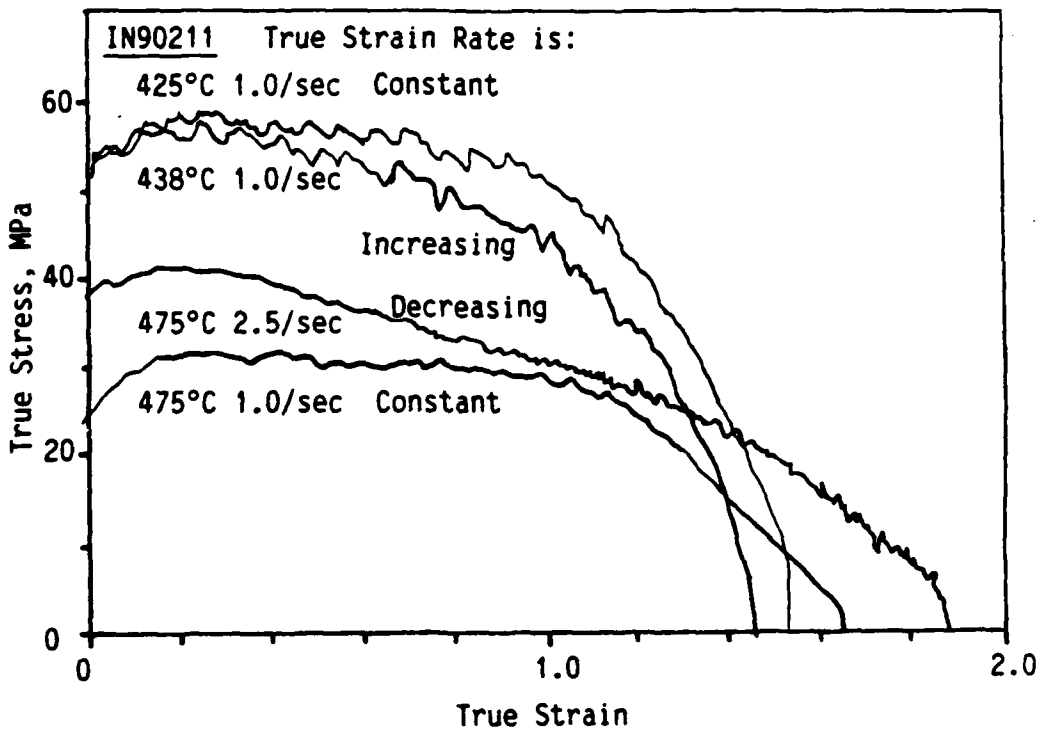
IN90211 True Strain Rate is:
425°C 1.0/sec Constant
438°C 1.0/sec
Increasing
Decreasing
475°C 2.5/sec
475°C 1.0/sec Constant
True Stress, MPa
60
40
20
0
0
1.0
2.0
True Strain

Fig. 2

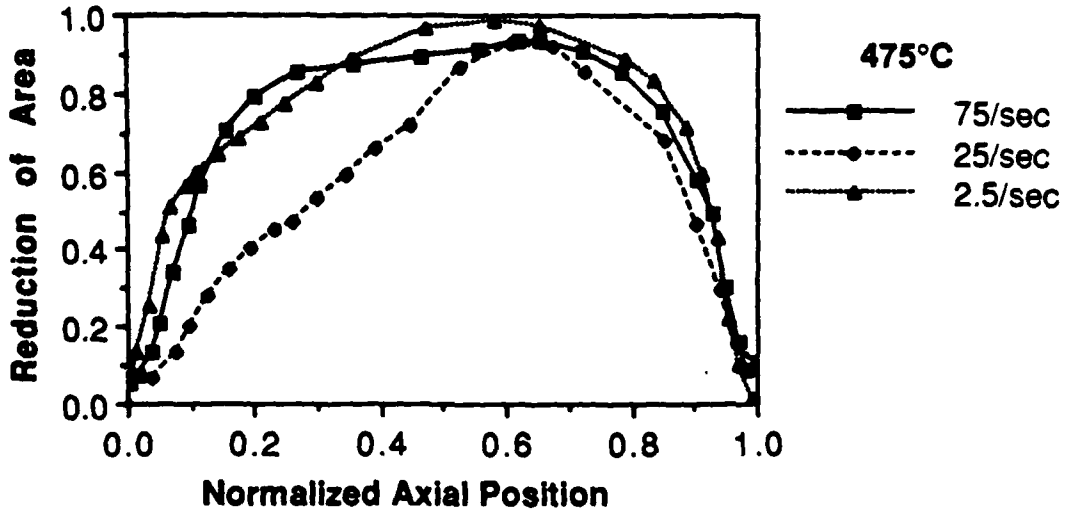
Reduction of Area
1.0
0.8
0.6
0.4
0.2
0.0
0.0
0.2
0.4
0.6
0.8
1.0
Normalized Axial Position
475°C
75/sec
25/sec
2.5/sec

Fig. 3

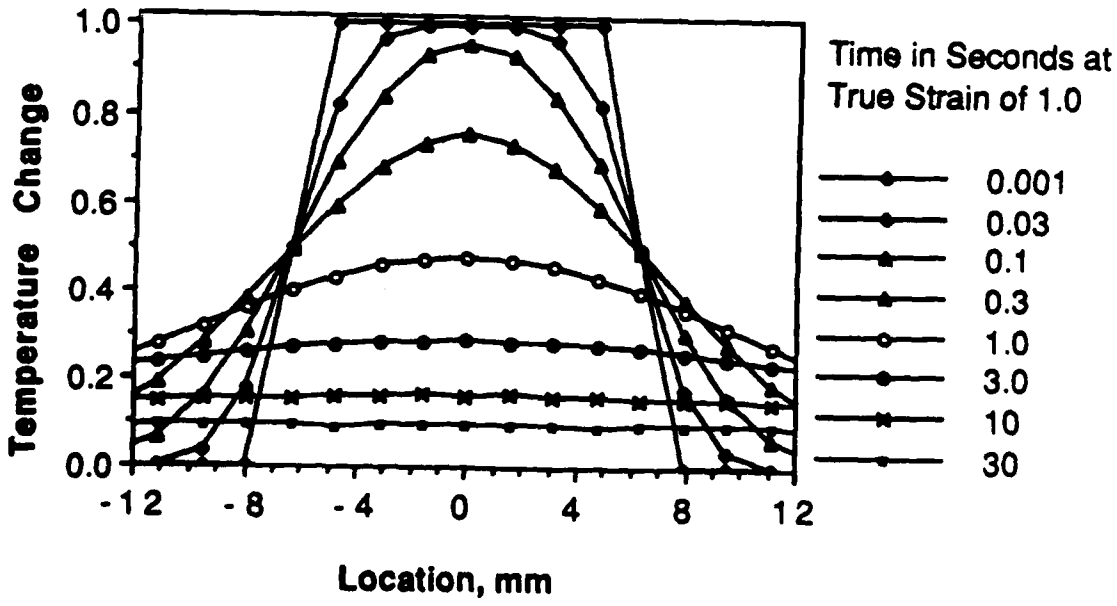
Temperature Change
1.0
0.8
0.6
0.4
0.2
0.0
-12
-8
-4
0
4
8
12
Location, mm
Time in Seconds at
True Strain of 1.0
0.001
0.03
0.1
0.3
1.0
3.0
10
30

Fig. 4

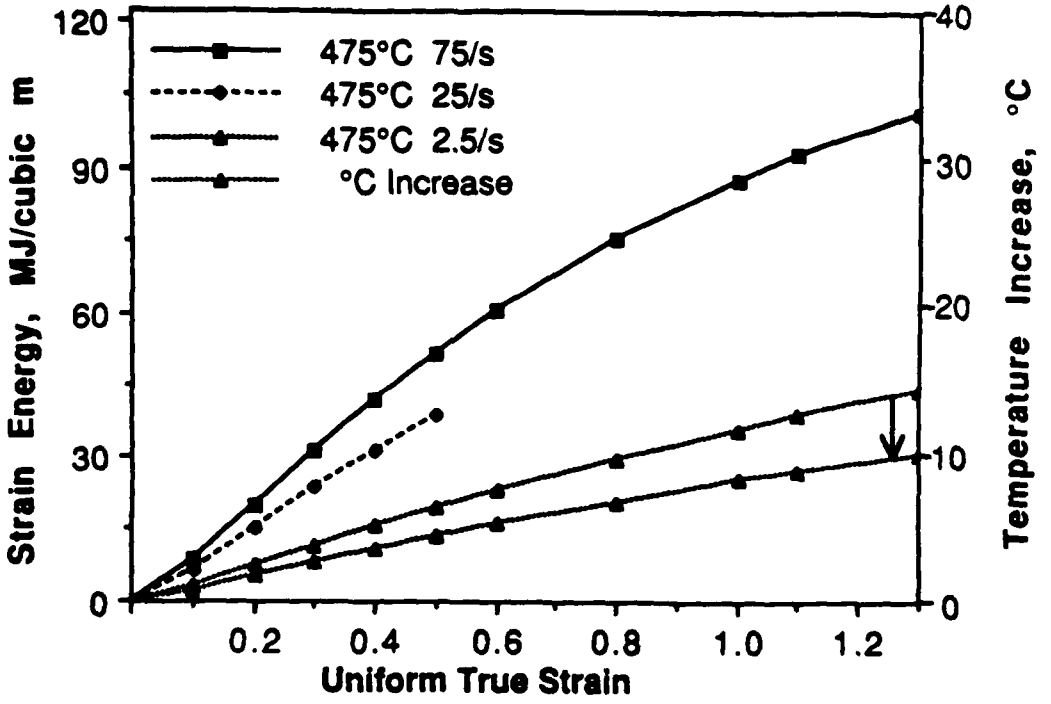
475°C 75/s
475°C 25/s
475°C 2.5/s
°C Increase
Strain Energy, MJ/cubic m
Temperature Increase, °C
Uniform True Strain
0
30
60
90
120
10
20
30
40
0.2
0.4
0.6
0.8
1.0
1.2

Fig. 5

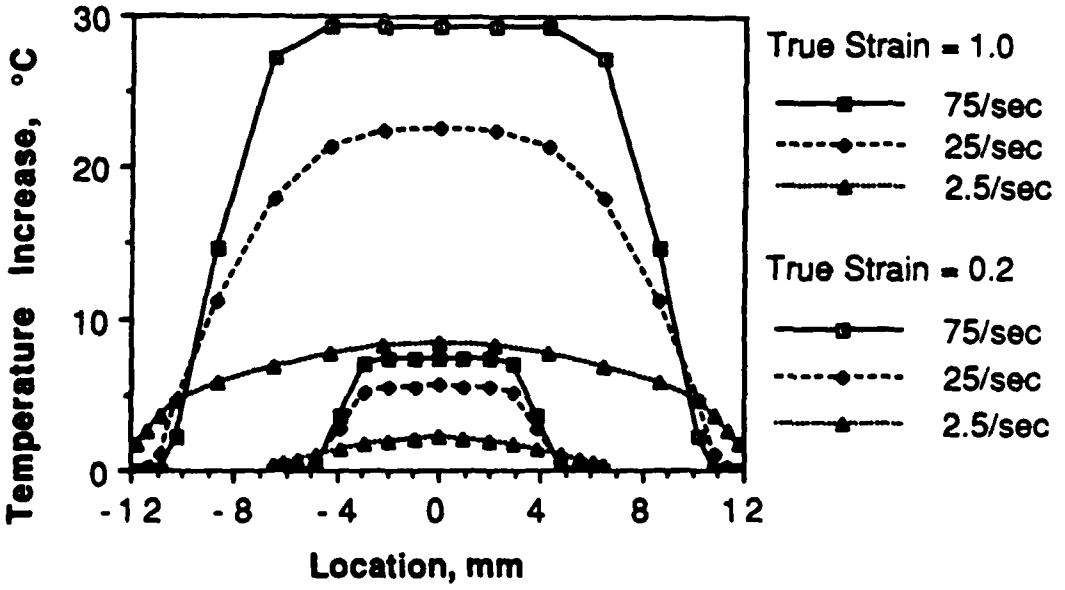
Temperature Increase, °C
Location, mm
True Strain = 1.0
75/sec
25/sec
2.5/sec
True Strain = 0.2
75/sec
25/sec
2.5/sec
0
10
20
30
-12
-8
-4
0
4
8
12

Fig. 6

III. CAVITATION OF MECHANICALLY ALLOYED ALUMINUM IN9021(1) AT 0.76-0.81 T_m

Cavitation that leads to fracture is a major concern for the practical use of materials for elevated temperature service under creep conditions and also for superplastic forming. Creep rupture life has been extended by thermo-mechanical processing in order to obtain elongated grains so as to minimize grain boundary area perpendicular to the tensile direction [1,2]. Superplasticity is possible under certain conditions when the alloy has a fine equiaxed grain size. Many superplastic alloys cavitate severely during deformation [3]. Methods that reduce or prevent cavitation have been developed, such as superposed hydrostatic pressure [4]. In addition, cavitation is minimal in two phase alloys where grains of the two phases have a different hardness (Ti and Pb-sn, and Al-Zn). The role of deformation mechanisms, grain boundary morphology, and diffusion are investigated to determine their role in cavitation of IN90211 (or the lack thereof).

A. Experimental Procedure and Results

Tensile specimens were made from processed sheet material produced by Novamet, Inc., and subsequently processed at the Research and Development Division of Lockheed Missiles and Space Co. Two lots of material were used, IN9021 sheet, and IN90211 extruded rod. The extruded rod was forge flattened and warm rolled to sheet 2.5 mm thick, annealed and water quenched. The IN90211 specimens used for superplasticity had a gage length of 6.3 mm, and were nominally 2.5 mm square. Longer specimens (51 mm) used for creep experiments were made

from 2 mm IN9021 sheet. Marks were made along the tensile axis with a pencil and photographed before and after deformation to permit accurate local strain and area reduction measurements. It was noted that more strain occurred in the thickness direction than in the width direction, as the area reduced. The overall stress-strain rate behavior was typical for superplasticity, exhibiting three deformation regimes, with maximum elongations occurring where the strain rate sensitivity is highest in the middle regime. These results are described in Section I.

Cavitation was investigated with optical microscopy, using a polished cross-section of the fractured specimen that included the fracture surface and the unstrained shoulder of the specimen. The width of the specimen where void density was measured was used with the photographs of the deformed specimen to determine the reduction of area corresponding with the region where cavity density was measured. At each location along the tensile axis 3 or 4 micrographs measuring 170 × 220 μm were made. Their positions away from the fracture surface were approximately 100, 450, (and in one case 800) μm from the fracture surface.

Cavitation in IN9021l was found to be less than 4% in the vicinity of fracture in the tensile specimens. Bar charts showing cavity distribution near the fracture surface are shown in Fig. 1. Cavitation for several specimens is tabulated in TABLE I. Cavitation is plotted as a function of true strain in Fig. 2. (The relationship between true strain and area reduction was used to determine the true strain near the fracture.) Cavity density was normalized by subtraction of the porosity in the shoulder of each specimen. The shoulder porosity varied considerably, from 0.01 to 0.16%, (counting voids larger than 2μm), as

specimen to specimen variation resulted from the fact that the rolled sheet was originally an extruded rod. Extremely fine features appearing as pin holes (on the order of 0.5 μm) were observed on many micrographs. If these are cavities, they are populous, providing as much as an additional 5% void fraction. Since these are of the order of the grain size, it is possible that they are grains pulled out during the polishing process, and not associated with cavitation.

The maximum cavity density found in a deformed specimen was 3-4% at the fracture surface of the specimens deformed above and below optimum superplastic strain rates at 475°C. Cavity density near the fracture surface at the optimum superplastic strain rate of 2.5/sec was 0.6%. Cavitation increased with temperature but so did the corresponding area reduction (and thus fracture strain). The distribution of cavities observed in specimens deformed at high rate differed from that at low rates, as illustrated in Fig. 1b. At the higher rate (75/sec), the cavity size distribution was characterized by numerous small cavities, with the largest contribution to the total cavity volume coming from cavities smaller than 7 μm. At the lower rate (0.0001/sec), the majority of the cavity volume came from cavities greater than 15 μm.

Grain morphology was determined from TEM observations. TEM specimens were prepared by grinding 3mm punched discs to 0.2 mm, and electrolytic thinning at -20°C in a 1:3 ratio of nitric acid and methanol. Specimens were taken both parallel and perpendicular to the rolling plane. Grains were found to be plate shaped, in accordance with the rolling plane, about 2-3 μm in diameter and about 0.3 μm thick (Fig. 3). Subgrain walls were nominally perpendicular to the rolling plane and grains had many submicron subgrains. Subgrain walls were low angle,

but exceptionally stable, since they were pinned by particles arising from the mechanical alloying process. The boundaries between platelets were typically high angle grain boundaries. These features were similar to other mechanically alloyed aluminum observations on IN9052, where the microstructure was described as having submicron subgrains [5].

Grain boundary sliding and fractography were investigated using the SEM. Some SEM specimens were coated with gold-palladium to improve resolution. Grain boundary sliding was observed on pre-polished surfaces of tensile specimens deformed superplastically. At lower superplastic strain rates (1-5/sec), the sliding entities were typically 2-3 μm platelets, but at higher strain rates, individual subgrain features were predominant. Fracture surfaces exhibited intergranular fracture for superplastic deformation. At strain rates below the superplastic regime, fracture surfaces exhibited an overall ductile-dimple mode, with intergranular fracture features on the surfaces of the dimples. The dimple size and spacing correlated well with observed cavities in the optical micrographs, indicating that cavity growth and inter-linkage preceded failure of low strain rate specimens. Fracture surfaces of extremely high strain rate (330/sec) specimens above the superplastic regime were similar to that of the low strain rate regime, but with fewer granular features observed on the dimple surfaces.

X-ray diffraction was done on an undeformed specimen and compared with a superplastically deformed specimen [6]. The results from X-ray analysis fall in two categories; d-spacings were smaller than standard pure aluminum powder samples, and the texture present in the undeformed specimen increased as a result of superplastic deformation. The smaller d-spacings resulted from the residual compressive stresses developed

around the oxide and carbide particles during cooling. The relative intensity of {200} planes was 1.3 times higher in the undeformed sample compared to the Al powder standard. This preferred orientation of {001} poles parallel to the rolling direction increases the number of {111} slip planes oriented along the planes of maximum shear stress. The superplastically deformed {200} peak intensity was twice the Al {200} powder standard, increasing the texture already present. This observation was unexpected as superplastic deformation often results in a decrease in texture due to the sliding and rotation of the grains.

B. DISCUSSION

Deformation mechanisms: An analysis of the IN9021(I) data indicated that the deformation mechanisms responsible for the superplastic deformation of IN9021 are both an n=3 slip mechanism in the grains and an n=2 grain boundary sliding mechanism (Section I). The homologous temperature is high enough that lattice diffusivity dominates, permitting relatively facile climb of dislocations over dispersions in the matrix. The threshold stresses associated with these particles are small, since diffusivity is high. Concurrently, the presence of Mg in the matrix limits dislocation progress by solute-drag. The lattice dislocations become extrinsic grain boundary dislocations when they reach the boundary, permitting grain boundary sliding. However, though all these processes occur, they do so in sequence, and the rate limiting step is dislocation glide in the interior of the matrix which happens to be the slowest of the sequential processes.

The sliding of clusters causes features similar to the inverted hourglass shape described by the core-mantle transitional model of Mayo

and Nix [7]. This model assumes that the deformation mechanism dominant in the interior (core) is different from the dominant mechanism near the grain boundary (mantle). Superplasticity results as a transition between the stresses where the core and mantle mechanisms occur in parallel, independent of each other, contrary to the result of the above analysis. This model requires a low dislocation density in the grain interior compared to the boundary, but the high dislocation density in the IN90211 grains ($>4\times10^{13}/m^2$) makes the model difficult to apply to IN9021. Therefore, if the above analysis is correct, then the inverted hourglass morphology of grain boundary sliding does not imply that the core mantle model accounts for the deformation mechanism. Mayo's core-mantle model was developed using two phase eutectic materials, while the IN90211 is a quasi-single phase material.

Grain Morphology: The shapes of grains in extruded ODS aluminum alloys has been investigated by Tweed, et.al. [8]. In an extruded ODS Al/Al_2O_3 alloy, about half of the boundaries were found to be low angle. A high percentage (80%) of the low angle boundaries were perpendicular to the extrusion/drawing direction, and similarly, 80% of high angle boundaries were parallel to the extrusion and drawing direction. Particles were found to pin the high angle boundaries in agreement with the Zener estimate. However, the particles pinned low angle boundaries more effectively than high angle boundaries. This can be rationalized in that low angle boundaries have about 1/5 of the energy of high angle boundaries. Using the lower boundary energy in the Zener estimate provided correlation with the observations. The low angle boundaries have more stability than high angle boundaries.

The above descriptions also applies to the trend of grain boundaries in IN9021(1), though no quantitative measurements were made. Numerous low angle boundaries were clearly observed in the specimen viewed in TEM perpendicular to the rolling direction. The platelets generally had high angle boundaries along the platelet interfaces, while the sub-boundaries within the platelets were usually low angle. Grain boundary clusters were observed to slide and rotate in IN9021, but the number of individual grain entities observed increased (and clusters decreased) in the specimen deformed at higher stress and strain rate, (Fig. 4), which apparently activated sliding on more of the boundaries that were stable at a lower stress and strain rate.

The low cavity nucleation in IN9021 can be rationalized by the grain morphology of IN9021. Creep in nickel based alloys has been shown to be much reduced when the number of boundaries oriented perpendicular to the tensile axis is minimized. This has been accomplished by making grains columnar [4,5]. IN9021 has some features of columnar grains in that the majority of the grain boundary surface perpendicular to the tensile axis consists of low angle boundaries, which resist cavity nucleation and sliding much more effectively than high angle boundaries. When these boundaries see a high enough stress to start sliding, more damage is done, increasing the nucleation sites for cavities. The larger thickness reduction than width reduction observed in the specimens indicates that strain in the material is anisotropic. If the grain boundary sliding process occurs primarily on the high angle boundaries, which are higher in energy and thus more mobile, then deformation can be visualized as a stack of coins with slippery interfaces. In this case, the shape of the coins does not need to

change substantially with strain, so as the coins slide over and under each other, the reduction in thickness can occur without the necessity of stretching the coin shape of the grain. Consequently, more overall strain takes place in the thickness direction than in the width direction, as illustrated in Fig. 5.

The microstructure of samples after deformation appeared to be similar to the undeformed microstructure. The grain size did not grow significantly. Particles consistently found in grain boundaries appear to stabilize the grain size. This high degree of thermal stability of the microstructure, and the lack of any observed dislocation free grains makes the possibility of dynamic recrystalization unlikely. Dynamic recrystallization can be beneficial for superplastic deformation, as an initially worked structure with lots of small angle boundaries can be converted to smaller grains with more high angle grain boundaries, which slide more effectively. This has been demonstrated in an Al-Li alloy, where initial fast straining causes dynamic recrystallization that provides an optimum small grain size for subsequent (lower strain rate) superplastic deformation [9]. However, the microstructure of IN9021 does not provide any evidence for dynamic recrystallization.

The increase in texture differs from the usual expectation in superplasticity, i.e., an increase in the randomness of grain orientation by the sliding and rotation of grains. The grain boundary sliding in IN9021 is different from that in usual superplastic materials since the platelet aspect ratio is not equiaxed. Since sliding in a direction perpendicular to the plane of the platelet is difficult, due to the low angle boundaries, hence the platelet grains remain in the same plane as they started. This accounts for the lack of a decrease in

texture, but not the observed increase. This increase in texture must result from platelet grains rotating within their planes to align themselves in the direction where (111) planes are aligned more favorably for slip. Consequently the platelet grains must become thinner and/or more elongated with strain. The surface in Fig. 4 clearly shows small rotations, and the appearance of inverted hourglass shapes is consistent with elongation of platelets along the tensile axis. Therefore, slip in the grains must occur during superplastic deformation. Slip can then help accommodate the compatibility problems at triple points, and thus help preclude cavitation.

Mechanism of Cavitation: Cavitation is minimized at optimum superplastic strain rates, unlike the results of other alloys [3]. Cavitation generally increases with grain boundary dislocation activity and grain size when grain boundary sliding is the rate controlling mechanism. In IN9021(1) grain boundary sliding is not rate limiting. The resistance to dislocation glide limits the rate of production of extrinsic grain boundary dislocations, which limits the rate of sliding. When sliding results in incompatibilities at triple points, particles or ledges in the boundary, stress concentrations can be accommodated by slip in the adjacent grain. When stress concentrations can be easily accommodated, cavitation is precluded. Furthermore, the vacancies that usually end up in cavities within the grain boundary, in the case of diffusion-limited growth process, have competition with the abundant cavity sources and sinks in the numerous particle interfaces and the large number of dislocations.

With increasing temperature, mobility of vacancies increases, so cavities that do start growing can attract vacancies and grow faster at

high temperatures than at lower temperatures (Fig. 1). This was evident in the large average cavity size near the fracture surface in the specimen strained at 0.0001/sec (475°C), where more than one hour elapsed before fracture. A similar volume of cavitation was seen at the high end of superplastic regime in the specimen deformed at 75/sec where fracture occurred shortly after 0.05 seconds. Cavities were smaller but more populous in the sample strained at high strain rate, where they had less time to grow by diffusive processes, but due to the higher stress, more nucleation sites were generated.

Fracture Surface: The fracture surfaces of non-superplastically deformed specimens showed cavitation similar to ductile-dimple fracture mode. Fracture surfaces of specimens deformed below the superplastic rates showed 20 μm pore spacing (Fig. 6a). Such spacing of large cavities was observed near the fracture surface in the optical micrographs as well. Intergranular fracture of superplastically deformed specimens is indicative of the grain boundary sliding process that accounts for the surface morphology and the large elongations (Fig. 6b). The mixed mode fracture at low strain rates consists of grain boundary separation, as in superplastic fracture, but the necks that strain preferentially between cavities deform at superplastic rates. At the bottom of the cavities, the individual grain surfaces are still seen, so even though cavities appear round, they have the surface features of the grains that border them. Thus fracture does not occur in the plasticity controlled manner observed in larger grain size metals, but rather by a mixture of intergranular separation followed by the overall growth of cavities from vacancy flux along grain boundaries. This scenario is consistent with the superplastic cavitation model of

Chokshi [10].

Intergranular failure predominates in the high temperature deformation of IN9021. Cavity spacing, when identified, is of the order of the grain size. The conditions for increasing intergranular character of failure follow directly from optimizing conditions for grain boundary sliding, which corresponds with optimum superplastic conditions. The conditions for increasing ductile failure phenomena are increasing strain rate above the optimum superplastic conditions and decreasing temperature. Under both of these conditions, mobility of grain boundary dislocations is insufficient for deformation to be accomplished only by grain boundary sliding, so accommodation is reduced and failure results from normal plastic failure.

C. CONCLUSIONS

Cavitation in superplastically deformed IN90211 is low, due to accommodation of stress concentrations occurring in grain boundary sliding by slip in the grains. Grain boundary sliding limited by matrix slip acts to retard grain boundary dislocation motion, permitting more time for accommodation to occur. The orientation of high angle grain boundaries parallel with the tensile axis and low angle boundaries perpendicular to the tensile axis provides minimal boundaries where cavities can grow in a tensile state of stress. This microstructural configuration resulted from extrusion and rolling texture. The inverted hour glass appearance of the grain boundary sliding can occur as a result of sliding of platelet shaped grains, and does not imply that a core-mantle deformation mechanism is necessarily operative. Superplastic elongations were obtained in an alloy that did not have

equiaxed grains, so equiaxed grains are not a necessary condition for superplastic elongations.

REFERENCES

1. B.A. WILCOX and A.H. CLAUER, Acta Metallurgica, 20, (1972), 743-757.

2. J.J. STEPHENS and W.D. NIX, Metallurgical Transactions 16A, (1985), 1307-1324.

3. B.P. KASHYAP and A.K. MUKHERJEE, Res Mechanica, 17, (1986), 293-355.

4. J. E. FRANKLIN, J. MUKHOPADHYAY and A. K. MUKHERJEE, Scripta Metallurgica, 22, (1988), 865-870.

5. M. OTSUKA, Y. ABE, and R. HORIUCHI, in Creep and Fracture of Engineering Materials and Structures, eds. B. Wilshire and R.W. Evans, The Institute of Metals, London, (1987), 307-317.

6. T.R. BIELER, Ph.D. dissertation, University of California at Davis, 1989.

7. M.L. MAYO and W.D. NIX, Acta Metallurgica, 37, (1989), 1121-2234.

8. C.J. TWEED, B. RALPH, and N. HANSEN, Acta Metallurgica, 32, (1984), 1407-14.

9. B.A. ASH and C.H. HAMILTON, Scripta Metallurgica, 22, (1988), 277-282.

10. A.H. CHOKSHI and T.G. LANGDON, International Conference on Superplasticity, Grenoble, Fr., eds. B.Baudelet and M. Suery, Editions du Centre National de la Recherche Scientifique, Paris, (1985), 2.1-2.15.

TABLES and FIGURES

TABLE I: CAVITATION AS A FUNCTION OF STRAIN AND STRAIN RATE

Location	Number and area of Cavities (μm)					Area	Density
Diameter:	1-2.5	2.5-5	5-7.5	7.5-10	>10		% *
Undef. No.	0	0	0	1	0	425°C, 0.0001/sec	
area	0	0	0	60	0	60	0.16
100 μm No.	17	13	9	3	1	(66% RA, 1.1 ε)	
area	21	144	276	180	99	720	1.92
Δ area	21	144	276	120	99	660	1.76
450 μm No.	10	10	1	1	0	(59% RA, 0.9 ε)	
area	12	111	31	60	0	214	0.57
Δ area	12	111	31	0	0	153	0.41
Undef. No.	8	0	0	0	0	425°C, 1/sec	
area	10	0	0	0	0	10	0.03
100 μm No.	9	7	3	0	0	(98.8% RA, 4.4 ε)	
area	11	77	92	0	0	180	0.64
Δ area	1	77	92	0	0	171	0.61
450 μm No.	24	9	0	0	0	(98.2% RA, 4.0 ε)	
area	30	99	0	0	0	129	0.46
Δ area	20	99	0	0	0	119	0.42
Undef. No.	13	0	0	0	0	425°C, 75/sec	
area	16	0	0	0	0	16	0.04
100 μm No.	23	10	3	0	0	(87% RA, 2.0 ε)	
area	28	111	92	0	0	231	0.61
Δ area	12	111	92	0	0	215	0.57
450 μm No.	15	2	0	0	0	(83% RA, 1.8 ε)	
area	18	22	0	0	0	41	0.11
Δ area	2	22	0	0	0	25	0.07
Undef. No.	16	2	0	0	0	475°C, 0.0001/sec	
area	20	22	0	0	0	42	0.11
100 μm No.	20	8	8	7	4	(73% RA, 1.3 ε)	
area	25	88	245	421	344	1224	3.25
Δ area	5	66	245	421	344	1182	3.14
450 μm No.	19	9	3	1	0	(70% RA, 1.2 ε)	
area	23	99	92	60	0	275	0.73
Δ area	4	77	92	60	0	233	0.62
Undef. No.	3	0	0	0	0	475°C, 75/sec	
area	4	0	0	0	0	4	0.01
100 μm No.	91	28	14	0	3	(93.3% RA, 2.71ε)	
area	112	309	430	0	298	1149	3.05
Δ area	108	309	430	0	298	1147	3.05
450 μm No.	94	23	11	6	0	(93.2% RA, 2.69ε)	
area	116	254	338	361	0	1068	2.84
Δ area	113	254	338	361	0	1064	2.83
800 μm No.	91	17	13	0	0	(93.2% RA, 2.69ε)	
area	112	188	399	0	0	699	1.86
Δ area	108	188	399	0	0	695	1.85

* Cavity measurement area is 37,620 μm^2, except for specimen deformed at 1/sec at 425°C, which had an area of 28220 μm^2

Fig. 1 a) The distribution of cavities near the fracture surface of a specimen deformed at 475°C, 0.0001/sec; b) The cavity size distribution differs depending upon strain rate (0.0001/sec and 75/sec). The cavity density at the fracture surface is 3% for both specimens.

Fig. 2 Cavity density (%) is plotted as a function of true strain (determined from reduction of area) for 425 and 475 °C.

Fig. 3 TEM dark field image showing plate-shaped grains with low angle boundaries. Rolling plane is perpendicular to page.

Fig. 4 Grain boundary sliding depends upon the applied stress, as indicated by a) grain cluster sliding at low stress and b) individual (sub)grains at high stress. Sliding of clusters appears similar to "the inverted hourglass" predicted by core-mantle theory of Mayo.

Fig. 5 Schematic diagram showing sliding of platelet shaped grains during superplastic elongation.

Fig. 6 Fracture surfaces of a) low strain rate and b) high superplastic strain rate specimens.

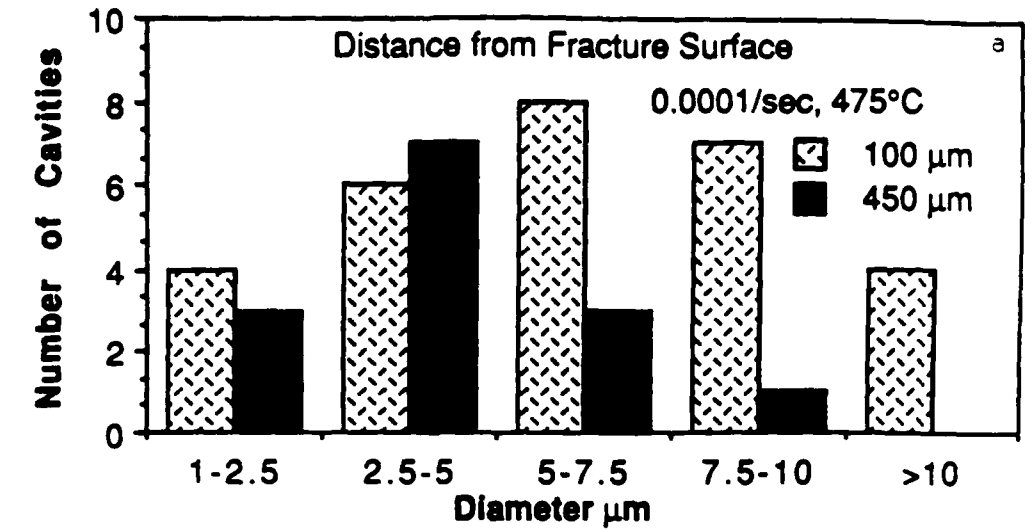
Distance from Fracture Surface
a
0.0001/sec, 475°C
100 µm
450 µm
Number of Cavities
0
2
4
6
8
10
1-2.5
2.5-5
5-7.5
7.5-10
>10
Diameter µm

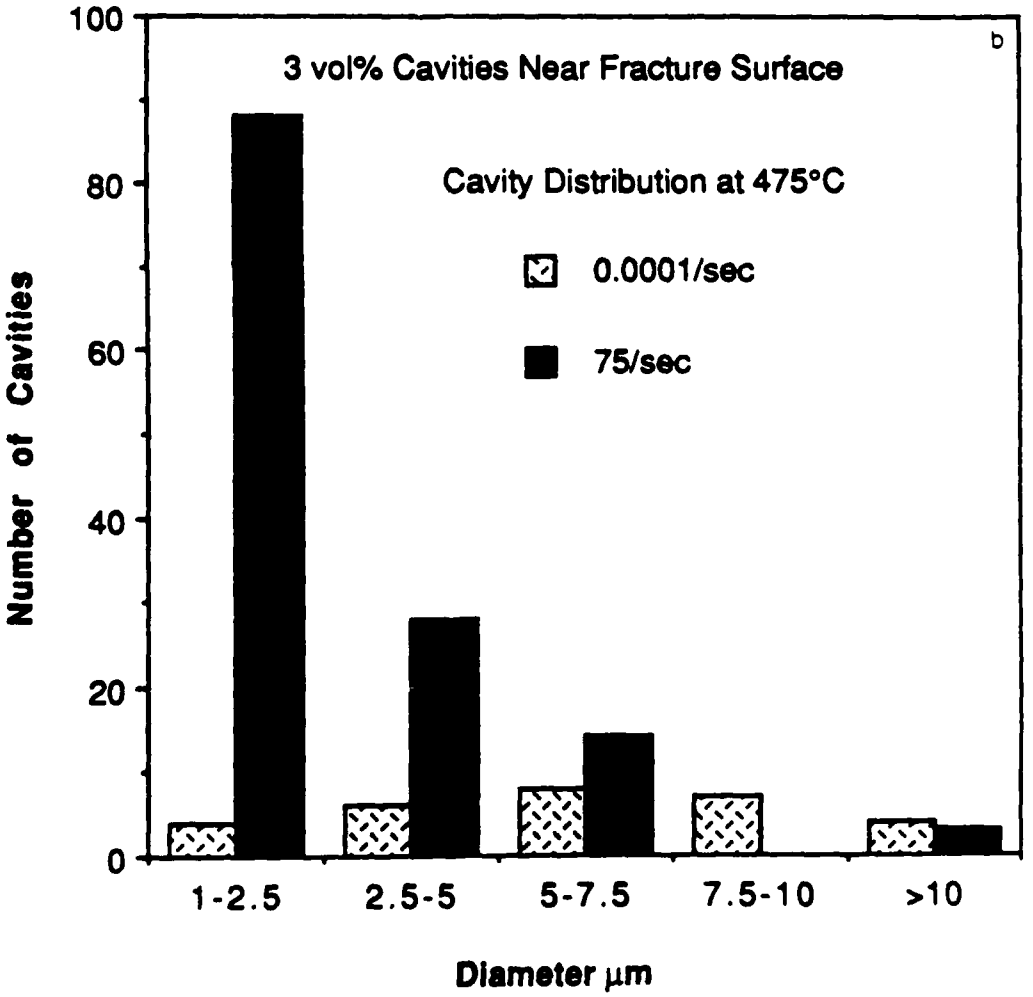
3 vol% Cavities Near Fracture Surface
b
Cavity Distribution at 475°C
0.0001/sec
75/sec
Number of Cavities
0
20
40
60
80
100
1-2.5
2.5-5
5-7.5
7.5-10
>10
Diameter µm

Fig. 1

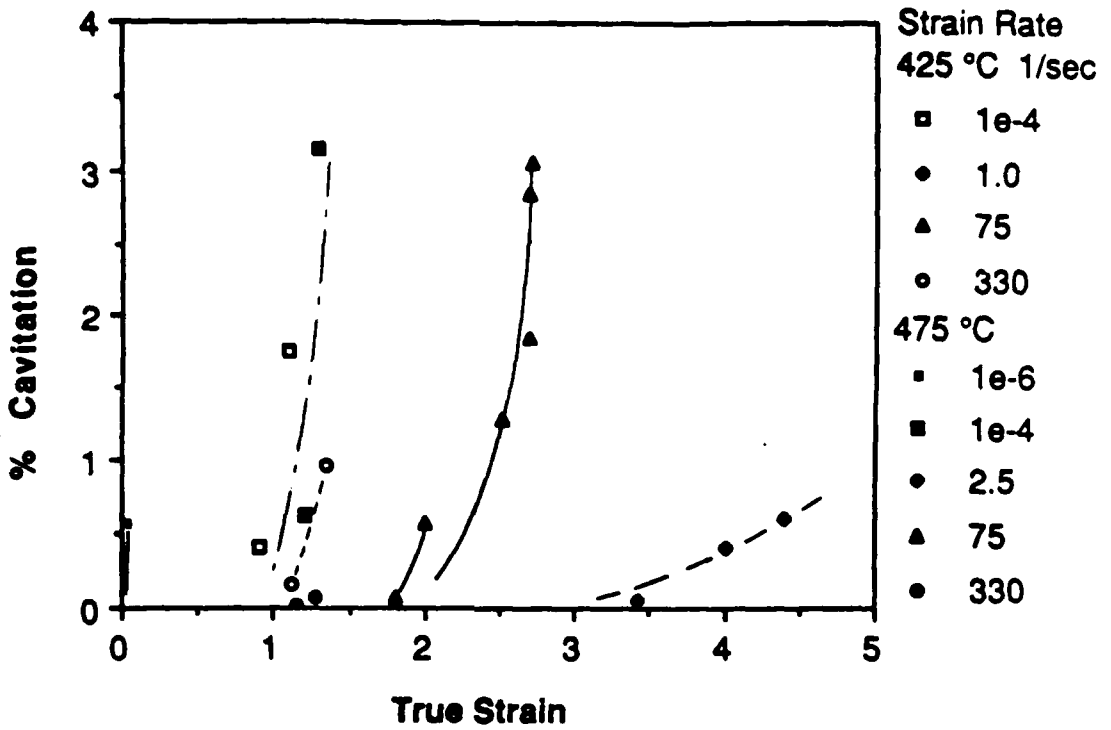

Fig. 2

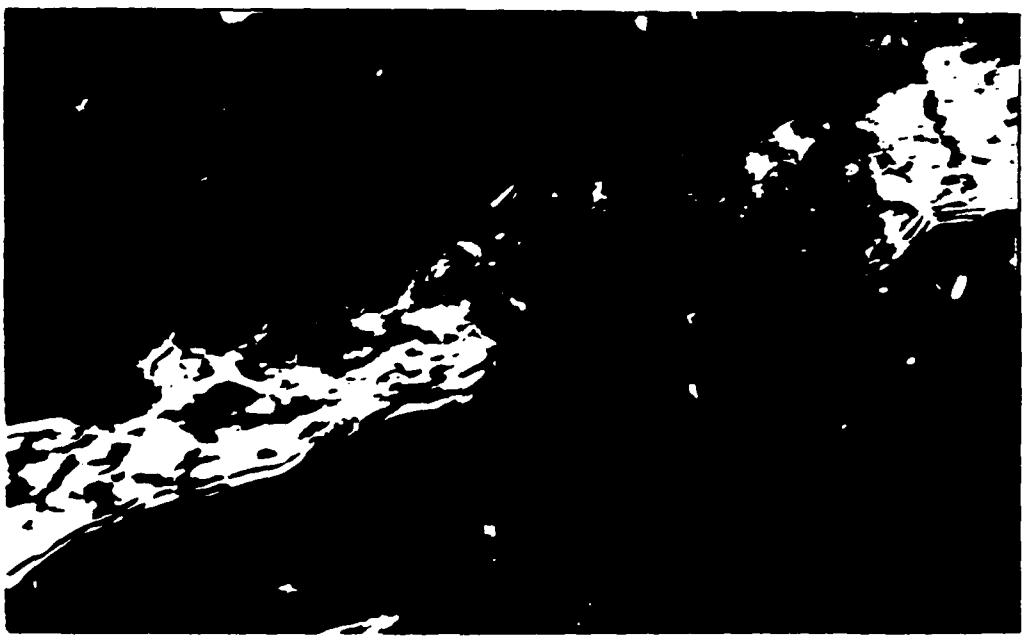

Fig. 3 200 nm

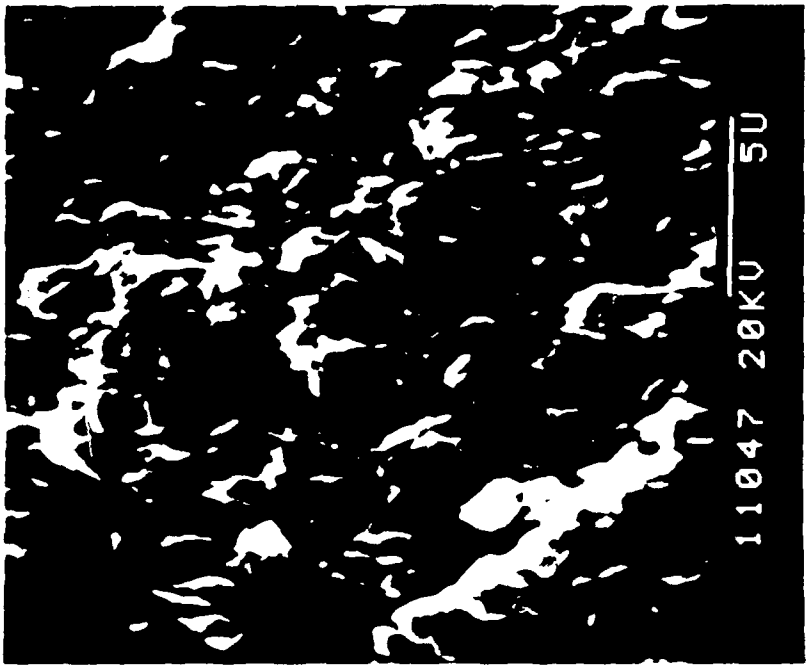

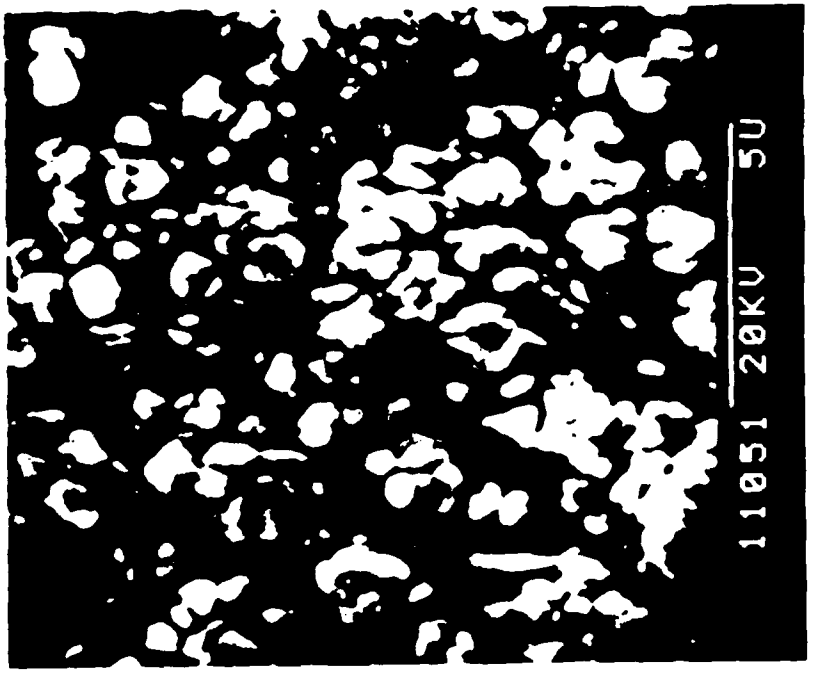

Fig. 4

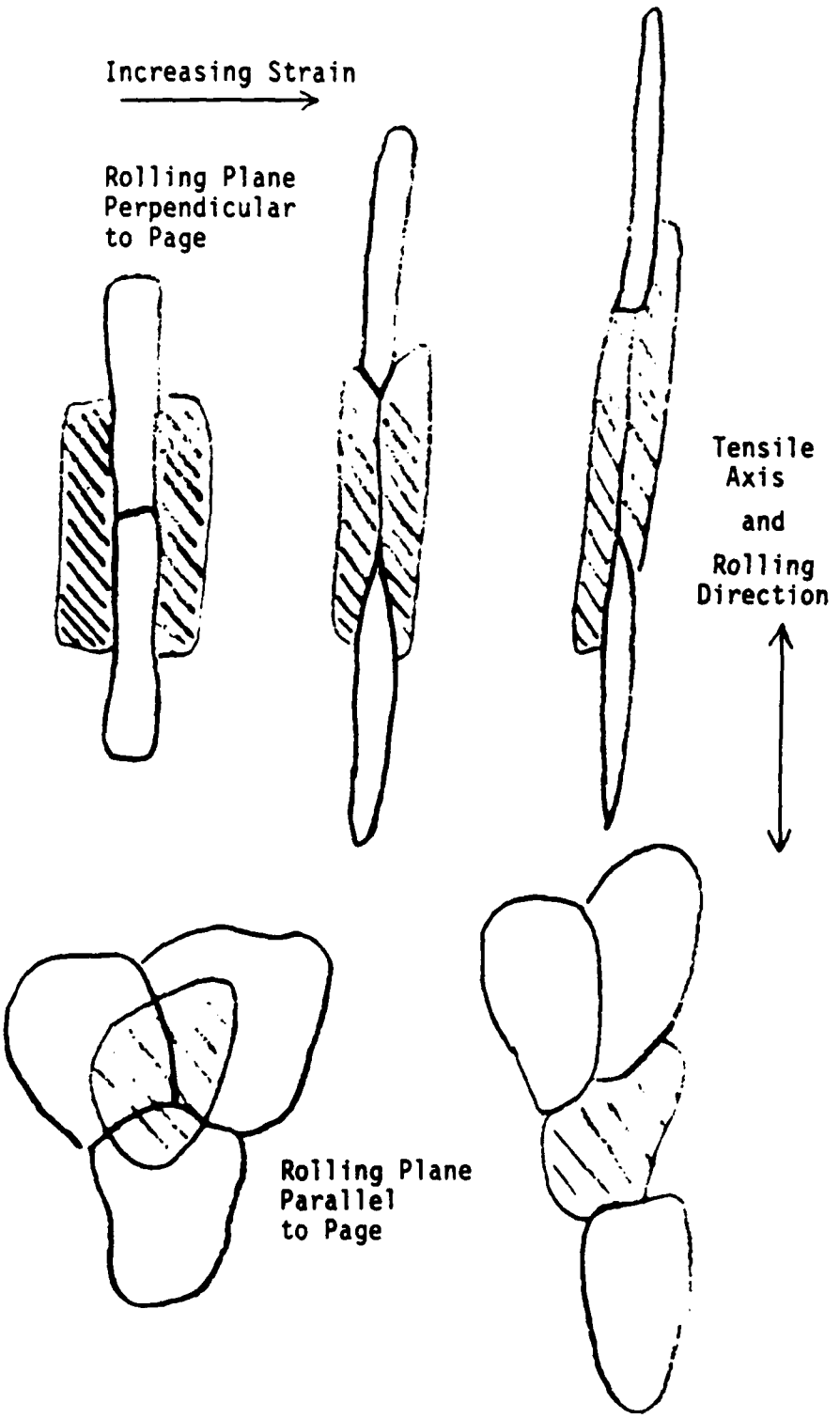
Increasing Strain
Rolling Plane
Perpendicular
to Page
Tensile
Axis
and
Rolling
Direction
Rolling Plane
Parallel
to Page

Fig. 5

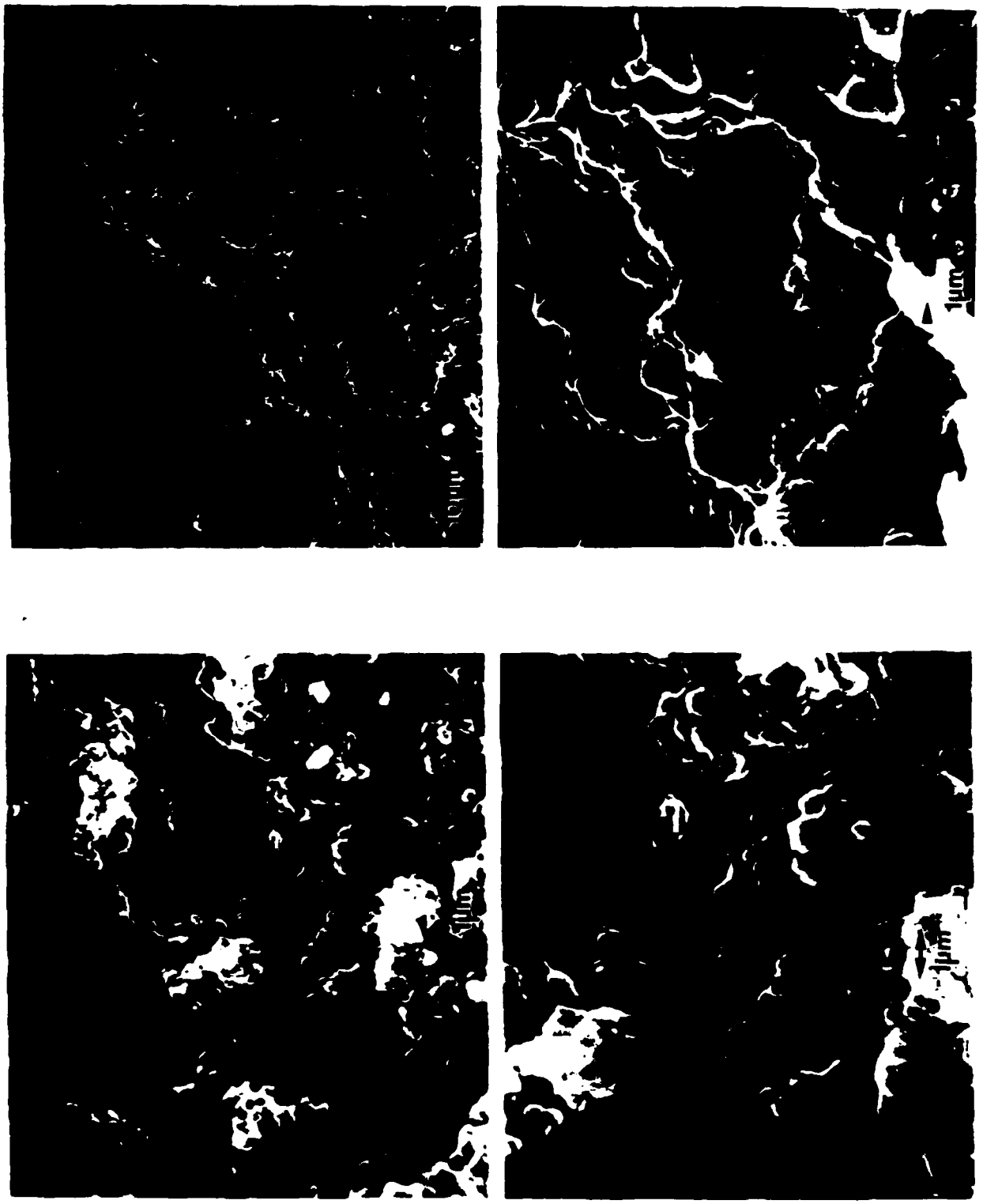

Fig. 6

IV. CUMULATIVE LIST OF PUBLICATIONS RESULTING FROM AFOSR SUPPORT

A-PUBLISHED

1980 1. LOW STRESS AND SUPERPLASTIC CREEP BEHAVIOR OF Zn-22% Al EUTECTOID ALLOY, A. Arieli, A. K. S. Yu, and A. K. Mukherjee, Metallurgical Transactions, Vol. 11A, pp. 181-191, 1980.

2. FACTORS AFFECTING THE MAXIMUM ATTAINABLE DUCTILITY IN A SUPERPLASTIC TITANIUM ALLOY, A. Arieli and A. Mukherjee, Materials Science and Engineering, Vol. 43, pp. 47-54, 1980.

3. HIGH-TEMPERATURE DIFFUSION-CONTROLLED CREEP BEHAVIOR OF THE Zn-22% Al EUTECTOID TESTED IN TORSION, A. Arieli and A. K. Mukherjee, Acta Metallurgica, Vol. 10, pp. 1571-1581, 1980.

4. AN EVALUATION OF THE EFFECTS OF CONCURRENT GRAIN GROWTH DURING SUPERPLASTIC FLOW OF THE Ti-6Al-4V ALLOY, A. Arieli, B. J. Maclean and A. K. Mukherjee, Proc. of the 4th Intnl. Conf. on Titanium, Kyoto, Japan, Ed. H. Kimura and O. Izumi, pp. 1047-1056, 1980.

5. TWO-AND THREE-DIMENSIONAL DEFORMATION MECHANISM MAPS FOR HIGH TEMPERATURE CREEP OF Zn-22% Al EUTECTOID ALLOY, A. Arieli and A. K. Mukherjee, Materials Science and Engineering, Vol. 47, pp. 113-120, 1980.

6. REPLY TO "A CRITICAL EVALUATION OF THE CONCEPT OF A UNIVERSAL PARAMETER TO UNIQUELY SPECIFY HIGH TEMPERATURE CREEP MECHANISMS," A. Arieli and A. K. Mukherjee, Scripta Metallurgica, Vol. 15, Sept. 81, p. 1053, 1980.

1983 7. THE EFFECT OF STRAIN AND CONCURRENT GRAIN GROWTH ON THE SUPERPLASTIC BEHAVIOR OF THE Ti-6Al-4V ALLOY, A. Arieli, B. J. McLean and A. K. Mukherjee, Res Mechanica, Vol. 6, pp. 131-159, 1983.

8. ELEVATED TEMPERATURE CAVITATION IN CREEP AND SUPERPLASTICITY OF Ti-6Al-4V ALLOY, G. Gurewitz, N. Ridley and A. K. Mukherjee, Proceedings of the International Conference on Fracture Mechanics, Nov. 1983, Pub. by the Chinese Soc. of Theoretical and Applied Mech., p. 898, Science Press, Beijing, China, 1983.

1984 9. MECHANICAL AND MICROSTRUCTURAL ASPECTS FOR OPTIMIZING THE SUPERPLASTIC DEFORMATION OF Ti-6Al-4V ALLOY, B. Hidalgo-Prada, G. Gurewitz and A. K. Mukherjee, Proceedings of Intn' Amer. Conf. on Mat. Tech., San Juan, Puerto Rico, Ed, D. Black, p. 18.1, 1984

1984 10. A METALLOGRAPHIC STUDY OF CAVITATION IN Ti-6Al-4V ALLOY, G. Gurewitz and A. K. Mukherjee, Advances in Fracture Research, Ed., S. R. Valluri, et al., Pergamon Press, Oxford, p. 2319-2324, 1984.

1985 11. CREEP AND DISLOCATION SUBSTRUCTURE, L. Bendersky, A. Rosen and A. K. Mukherjee, Invited Review, International Metals Review, Vol. 30, p. 1, 1985.

12. THE STRAIN RATE SENSITIVITY VALUES IN SUPERPLASTIC DEFORMATION, G. Gurewitz and A. K. Mukherjee, Materials Science and Engineering, Vol. 70, p. 191-196, 1985.

13. ON THE NEW MODELS OF SUPERPLASTIC DEFORMATION, B. P. Kashyap and A. K. Mukherjee, Proceeding of International Conference on Superplasticity, Grenoble, France, pp. 4.1-4.31, Sept. 1985.

14. MICROSTRUCTURAL EVOLUTION DURING SUPERPLASTIC DEFORMATION IN A Ni-MODIFIED Ti-6Al-4V ALLOY, B. Hidalgo-Prada and A. K. Mukherjee, Scripta Metallurgica, Vol. 19, pp. 1235-1239, 1985.

15. SUPERPLASTICITY-CORRELATION BETWEEN STRUCTURE AND PROPERTIES, M. Suery and A. K. Mukherjee, Creep Behavior of Crystalline Solids, ed. B. Wilshire, Pineridge Series on Progress in Creep and Fracture, Pineridge Press, Swansea G.B., pp. 137-200, 1985

16. CORRELATION BETWEEN MECHANICAL PROPERTIES AND MICROSTRUCTURE IN A NI-MODIFIED SUPERPLASTIC Ti-6Al-4V ALLOY, B. Hidalgo-Prada and A.K. Mukherjee, Proc. of Intnl. Conf. of Strength of Metals and Alloys-7, Montreal Canada, ed. H.J. McQueen et al., Vol. 2, pp. 835-840, 1985.

1986 17. CAVITY NUCLEATION IN 7475 AL ALLOY, M. K. Rao and A. K. Mukherjee, Scripta Met., Vol. 20, pp. 411-414, 1986.

18. REVIEW: CAVITATION BEHAVIOR DURING HIGH TEMPERATURE DEFORMATION OF MICROGRAINED SUPERPLASTIC MATERIALS, B. P. Kashyap and A. K. Mukherjee, Invited review, Res Mechanica, Vol. 17, pp. 293-355, 1986.

19. SUPERPLASTIC DEFORMATION BEHAVIOR IN INGOT AND POWDER METALLURGICALLY PROCESSED Al-Li BASED ALLOYS, M.C. Pandey, J. Wadsworth and A.K. Mukherjee, Materials Science and Engineering, Vol. 80, No. 2, pp. 169-179, 1986.

20. ON THE TRANSITION FROM SUPERPLASTIC TO NON-SUPERPLASTIC DEFORMATION AT HIGH STRAIN RATES, Atul Chokshi and Amiya Mukherjee, Scripta Met, Vol. 20, pp. 1771-1774, 1986.

1987 21 ON THE EVALUATION OF PARAMETERS OF THE CONSTITUTIVE EQUATION FOR 7475 AL ALLOY,
M. Rao and A. K. Mukherjee, Journal of Materials Science, Vol. 22, pp. 459-465, 1987.

22. SUPERPLASTIC DEFORMATION IN AN AL-Li ALLOY,
A. Chokshi, A.K. Mukherjee, Proc. of International Conference on Metallurgy and Materials Science, pp. 265-272, 1987, Ed. S.I. Andersen, et al., Denmark.

1988 23. EFFECT OF HYDROSTATIC PRESSURE ON HIGH TEMPERATURE FAILURE IN SUPERPLASTIC ALUMINUM ALLOYS,
A.H. Chokshi, J.E. Franklin and A.K. Mukherjee, Mechanical Behavior of Materials, Ed. M.G. Yan, et al., Vol. 1, pp. 461-468, 1987.

23. MICROSTRUCTURAL EVIDENCE FOR DYNAMIC RECRYSTALLIZATION DURING SUPERPLASTIC DEFORMATION,
Atul H. Chokshi, Jeffrey Wadsworth and Amiya K. Mukherjee, Scripta Met., Vol. 21, p 1347-1351, 1987.

1988 24. ON THE INTER-DEPENDENCE OF GRAIN BOUNDARY PHENOMENON AND SUPERPLASTIC DEFORMATION,
B.P. Kashyap and A.K. Mukherjee, Fundamentals of Diffusion Bonding, Ed. Y. Ishida, Elsevier, Amerstadam P. 397-420, 1988.

25. A TOPOLOGICAL STUDY OF SUPERPLASTIC DEFORMATION IN AN AL-Li ALLOY WITH A BIMODAL GRAIN SIZE DISTRIBUTION,
A. H. Chokshi and A. K. Mukherjee, Metallurgical Transactions, Vol. 19A, p. 1621, 1988.

26. CREEP CAVITY GROWTH FROM TRITIUM-INDUCED HELIUM BUBBLES IN NICKEL, J. M. Mintz and A. K. Mukherjee, Metallurgical Transactions, Vol. 19A, pp. 821-827, 1988.

27. SUPERPLASTIC-LIKE BEHAVIOR AT HIGH STRAIN RATES IN A MECHANICALLY ALLOYED ALUMINUM,
T. R. Bieler, T. G. Nieh, J. Wadsworth and A. K. Mukherjee, Scripta Met., Vol. 22, pp. 81-86, 1988.

28. SUPERPLASTICITY IN A MECHANICALLY ALLOYED MATRIX,
T. R. Bieler, and A. K. Mukherjee, Invited paper, XXII International Metallurgy Congress, Bologna, Italy, Vol. 1, pp. 485-503, 1988.

29. SUPERPLASTICITY IN SILICON CARBIDE REINFORCED ALUMINUM AND MECHANICALLY ALLOYED ALUMINUM AEROSPACE ALLOYS,
A. H. Chokshi, T. R. Bieler, T. G. Nieh, J. Wadsworth and A. K. Mukherjee, Superplasticity in Aerospace, Ed. H. C. Heikkenen, et al., A.I.M.E., Warrendale, PA., pp. 229-245, 1988.

30. CAVITATION FAILURE IN SUPERPLASTIC ALLOYS,
A. H. Chokshi and A. K. Mukherjee, Superplasticity in Aerospace, Ed. H. C. Heikkenen, et al., A.I.M.E., Warrendale, PA., pp. 167-182, 1988.

1988 31. ON THE EFFECTS OF HYDROSTATIC PRESSURE ON MECHANICAL PROPERTIES OF 7475 ALUMINUM ALLOY,
J. E. Franklin, J. Mukhopadhyay and A. K. Mukherjee, Scripta Metallurgica, Vol. 22, pp. 865-870, 1988.

32. THE SUPERPLASTIC-LIKE CHARACTERISTICS OF A SILICON CARBIDE WHISKER REINFORCED ALUMINUM COMPOSITE,
A. H. Chokshi, T. G. Nieh, J. Wadsworth and A. K. Mukherjee, Strength of Metals and Alloys, Ed. P. O. Kettunen, et al., Pergamon Press, Vol. 1, p. 301, 1988.

33. SUPERPLASTIC BEHAVIOR OF MECHANICALLY ALLOYED ALUMINUM IN90211,
T. R. Bieler and A. K. Mukherjee, Strength of Metals and Alloys, Ed. P. O. Kettunen, et al., Vol. 1, pp. 289-294, 1988.

34. THRESHOLD STRESS AND SUPERPLASTIC BEHAVIOR OF MECHANICALLY ALLOYED ALUMINUM IN90211,
T. R. Bieler and A. K. Mukherjee, Mechanical and Physical Behavior of Metallic and Ceramic Composites, Ed. S. I. Anderson, et al., Riso, Denmark, pp. 297-302, 1988.

35. PARTICLE CHARACTERIZATION AND CAVITY NUCLEATION DURING SUPERPLASTIC DEFORMATION IN AL-Li BASED ALLOYS,
M. C. Pandey, J. Wadsworth and A. K. Mukherjee, Journal of Materials Science, Vol. 23, p. 3509, 1988.

36. ENHANCED PLASTICITY OF MECHANICALLY ALLOYED ALUMINUM IN90211,
T. R. Bieler, T. G. Nieh, J. Wadsworth and A. K. Mukherjee, Symposium I on "Interfacial Structure, Properties and Design, Materials Research Society, Vol. 120, pp. 137 142, 1988

37. THE ROLE OF CAVITATION IN THE FAILURE OF SUPERPLASTIC ALLOYS,
A. H. Chokshi and A. K. Mukherjee. In: Superplasticity and Superplastic Forming, Eds. C.H. Hamilton and N.E. Paton, TMS-AIME, Warrendale, PA, pp. 149-159, 1989.

38. HIGH RATE SUPERPLASTIC BEHAVIOR OF MECHANICAL ALLOYED ALUMINUM IN90211,
T. R. Bieler, T. G. Nieh, J. Wadsworth and A. K. Mukherjee. In: Superplasticity and Superplastic Forming, Eds. C. H. Hamilton and N.e. Paton, TMS-AIME, Warrendale, PA., pp. 161-165, 1989.

B. PAPERS AND BOOKS ACCEPTED FOR PUBLICATION, SUBMITTED AND IN PREPARATION

A. K. Mukherjee

B-1 IN PRESS

1. THE CAVITATION AND FRACTURE CHARACTERISTICS OF A SUPERPLASTIC Al-Cu-Li-Zr ALLOY,
A.H. Chokshi and A.K. Mukherjee, Materials Science and Engineering.

2. THE ROLE OF GRAIN BOUNDARIES IN THE DEFORMATION AND FAILURE OF A SUPERPLASTIC Al-Li ALLOY,
A.H. Chokshi and A.K. Mukherjee, MRS Symposium I on "Interfacial Structure, Properties and Design", Reno Nevada, 1988.

B-2 SUBMITTED

1. AN ANALYSIS OF CAVITY NUCLEATION IN SUPERPLASTICITY,
A.H. Chokshi and A.K. Mukherjee, submitted to Acta Metallurgica.

2. THE INFLUENCE OF HYDROSTATIC PRESSURE ON GRAIN BOUNDARY SLIDING IN SUPERPLASTICITY: IMPLICATIONS FOR CAVITATION,
A.H. Chokshi and A.K. Mukherjee, submitted to Acta Metallurgica, 1988.

3. THE ROLE OF HYDROSTATIC PRESSURE IN THE CAVITATION FAILURE OF A SUPERPLASTIC ALUMINUM-LITHIUM ALLOY,
A.H. Chokshi and A.K. Mukherjee, submitted for publication in a Memorial Monograph by the American Geophysical Union.